

WENDy for Nonlinear-in-Parameters ODEs

Nic Rummel¹, Daniel A. Messenger², Stephen Becker¹, Vanja Dukic¹, and David M. Bortz¹

¹ Department of Applied Mathematics, University of Colorado, Boulder, CO 80309-0526

² Theoretical Division, Los Alamos National Laboratory, Los Alamos, NM 87545

E-mail: `nic.rummel@colorado.edu`, `david.bortz@colorado.edu`

Abstract. The Weak-form Estimation of Non-linear Dynamics (WENDy) algorithm is extended to accommodate systems of ordinary differential equations that are nonlinear-in-parameters. The extension rests on derived analytic expressions for a likelihood function, its gradient and its Hessian matrix. WENDy makes use of these to approximate a maximum likelihood estimator based on optimization routines suited for non-convex optimization problems. The resulting parameter estimation algorithm has better accuracy, a substantially larger domain of convergence, and is often orders of magnitude faster than the conventional output error least squares method (based on forward solvers).

The [WENDy.jl](#) algorithm is efficiently implemented in Julia. We demonstrate the algorithm's ability to accommodate the weak form optimization for both additive normal and multiplicative log-normal noise, and present results on a suite of benchmark systems of ordinary differential equations. In order to demonstrate the practical benefits of our approach, we present extensive comparisons between our method and output error methods in terms of accuracy, precision, bias, and coverage.

Keywords : Parameter Estimation, Weak Form Learning, Maximum Likelihood Estimation

Submitted to: *Inverse Problems*

1. Introduction

Parameter estimation and inference for differential equations (DEs) remains a challenging problem despite the many sophisticated algorithms that have been developed over the years [34]. Precursors to modern approaches can be traced back to the dawn of computational science in the 1950's and 1960's [18] and have been historically categorized into Output Error (OE) or Equation Error (EE) approaches [30, 31].

The more common OE-based methods first propose a candidate parameter value, numerically compute an approximate solution, compare with data, and then iterate the parameter proposal until the comparison metric drops below a specified threshold. OE methods have come to dominate the parameter estimation literature partially because they can leverage existing numerical simulation and nonlinear optimization approaches. However, the cost functions commonly resulting from nonlinear differential equation systems often exhibit multiple modes and ridges, and thus convergence to globally optimal and unique parameter values frequently requires long run times and careful diagnostic monitoring [11, 26, 52], and assessment of the impact of hyperparameter choices from the DE solver and optimization algorithm on the parameter estimates themselves [44]. These practical challenges have motivated alternative approaches with reduced reliance on forward-based solvers, including likelihood-free sequential Monte Carlo methods [63], local approximations [10], manifold-constrained Gaussian processes [67, 68], and weak-form methods [5, 7, 20].

EE-based estimation involves substituting data directly into a model and minimizing the norm of the resulting residual. If the model equation is linear in the parameters (LiP), the resulting problem is a simple linear regression. This category also encompasses a variety of extensions that minimize transformed versions of the residual. For example, a Fourier Transform of the model equations results in a Fourier Error (FE) method. FE-methods are efficient, but that efficiency is (generally) limited to models that are LiP. Conversely, if the model is *nonlinear* in the parameters (NiP), this results in a nonlinear regression problem, necessitating an iterative scheme for the optimization. The NiP EE-based scenario has not received nearly as much attention as the LiP case, forming a major motivation for our efforts here.

1.1. Weak Form System Identification

Another EE extension involves converting the model equation to its weak form, i.e., convolving with a compactly supported test function, φ , and integrating by parts. Researchers have explored several forms including those based upon piecewise [33] and Hermite [62] polynomials, Fourier [48] and Hartley [47] Transforms, and Volterra linear integral operators [49, 50]. However, while it was known that the choice of φ impacts the estimation and inference accuracy, only recently have there been precise derivations of the impact of test function hyperparameters on the solution [5, 19, 35, 36, 38].

Historically, weak form versions of EE-based parameter estimation have been proposed repeatedly over the years, originally in the aerospace engineering literature

[32, 33, 58, 59] and later (independently) explored in statistics [7, 20] and nonlinear dynamics [5, 28]. Notably, in 1965, Loeb and Cahen [32, 33] introduced their method, called the *Modulating Function Method* (MFM). The MFM-based research was active for many years, particularly in the control literature, but the field became mostly dormant by the end of the twentieth century.

Starting in 2010, research in two independent areas led to a resurgence in interest in weak form system identification. Janiczek noted that a generalized version of integration-by-parts could extend the traditional MFM to work with fractional differential equations [23]. This discovery led to a renewed (and sustaining) interest by several control engineering researchers, c.f. [2, 24, 29].

The second independent line of weak form research arose out of the field of sparse regression-based equation learning. The seminal work in this area is the Sparse Identification of Nonlinear Dynamics (SINDy) methodology, originally proposed in 2016 for ODEs in [8] and in 2017 for PDEs in [55, 57]. It is a data-driven modeling approach that learns both the form of the differential equation and the parameters directly from data. While incredibly successful, the original SINDy method was not robust to noise. Subsequently, several researchers independently noticed the value in casting equations in the weak form [19, 35, 36, 46, 66]. In particular, we note that the Weak form Sparse Identification of Nonlinear Dynamics (WSINDy) method proposed in [35, 36] clearly demonstrates the noise robustness and computational efficiency of a weak form approach to equation learning. We direct the interested reader to recent overviews [6, 41] and further WSINDy extensions [37, 39, 40, 42, 56, 64].

Lastly, we note that all the above EE-based approaches rarely address the fact that the data appears in all terms of the EE regression, i.e., in the matrix and the vector. This class of problems is known as an Errors-in-Variables problem [12] and can be addressed using methods from the generalized least squares literature. In our previous work [5], we proposed using an iteratively reweighted least squares approach (IRLS) which repeatedly solves the EE regression, updating the covariance at each step. In what follows, we denote the original WENDy algorithm as WENDy-IRLS.

1.2. Contribution

The current work extends the WENDy-IRLS algorithm (as described in [5]) to estimate parameters in a broader class of differential equation models. Our novel extension, called WENDy-MLE, can estimate parameters for systems of ordinary differential equations that are NiP. Furthermore, we extend the framework of our derivation beyond additive Gaussian noise, and now can explicitly address multiplicative log-normal noise. The algorithm is based on likelihood function optimization, and designed to find the maximum likelihood estimate of the parameters. This is done via an efficient implementation in Julia [4] with analytic computation of first and second order derivatives of the likelihood. Through numerical results, we demonstrate that the algorithm converges to accurate estimates of the parameters more often than a

conventional forward solver-based least squares method.

The paper is structured as follows: Section 2 describes the mathematical derivation of the weak form, noise models, maximum likelihood estimation and analytic computation of derivatives. Section 3 presents a brief overview of the implementation of the WENDy-MLE algorithm and the numerical results from applying our framework to specific examples of systems of ordinary differential equations, comparing to a baseline forward simulation-based solver, and examining robustness to noise and initialization and availability of data. We conclude this work in Section 4 with a discussion of strengths and weaknesses in our approach including how our approach compares with other state-of-the-art methods. Concluding remarks are made in Section 5, and acknowledgements are made in Section 6.

2. WENDy-MLE Algorithm: Mathematical Framework

This section lays out the mathematical foundation and needed assumptions for the new WENDy-MLE algorithm. It first describes the class of differential equations and noise for which the algorithm is applicable. We then present the distribution of the weak-form residual and the corresponding likelihood function under the Gaussian noise assumption. Furthermore, we show how to compute first and second-order derivative for the analytic likelihood, and how to utilize that information in the underlying optimization algorithms. Finally, we extend the framework to the case of multiplicative log-normal noise. We provide additional discussion, as well as simplifications and computational speedups available when the model is LiP, in [Appendix B](#).

To set notation, we assume that the data of the dynamical system is governed by a fully-observed D -dimensional system of ordinary differential equations (ODE) of the form

$$\dot{\mathbf{u}}(t) = \mathbf{f}(\mathbf{p}, \mathbf{u}(t), t) \quad (1)$$

where $\mathbf{u}(t) \in \mathcal{H}^1((0, T), \mathbb{R}^D)$ is the function state variable at time $t \in [0, T]$; we typically drop the t dependence and write $\dot{\mathbf{u}} = \mathbf{f}(\mathbf{p}, \mathbf{u}, t)$ for short. The driving function \mathbf{f} is (possibly nonlinearly) parameterized by a finite set of unknown parameters $\mathbf{p} \in \mathbb{R}^J$ that we wish to recover, and \mathbf{f} may also be nonlinear in \mathbf{u} and t . It is required that \mathbf{f} be twice continuously differentiable with respect to \mathbf{p} and \mathbf{u} . Note that we use bold lowercase variables to indicate vectors and vector-valued functions, and bold upper case to indicate matrices and matrix-valued functions. We use $\|\cdot\|$ to denote the 2-norm for vectors and the operator norm for matrices unless otherwise specified.

2.1. The Weak Form

To implement the WENDy-MLE approach, we first convert Equation (1) from strong to weak form. This is done by taking the $L^2((0, T))$ inner product, $\langle \cdot, \cdot \rangle$, with an analytic compactly supported test function, $\varphi(t) \in \mathcal{C}_c^\infty((0, T), \mathbb{R}^D)$. In this work, multivariate

test functions are chosen to be of the form $\varphi(t) = \mathbf{1}_D \varphi(t)$ where $\varphi(t) \in \mathcal{C}_c^\infty((0, T), \mathbb{R})$ ‡. The weak form now becomes

$$\langle \varphi, \dot{\mathbf{u}} \rangle = \langle \varphi, \mathbf{f}(\mathbf{p}, \mathbf{u}, t) \rangle. \quad (2)$$

Because the test functions have compact support, integration by parts allows movement of the derivatives onto the test functions:

$$-\langle \dot{\varphi}, \mathbf{u} \rangle = \langle \varphi, \mathbf{f}(\mathbf{p}, \mathbf{u}, t) \rangle. \quad (3)$$

Formally, to satisfy the weak form, a solution must solve the Equation (2) (and equivalently Equation (3)) for all possible test functions. For computational reasons, a finite set of test functions, $\{\varphi_k\}_{k=1}^K$, is chosen. The strategy for choosing an optimal set of test functions for a specific problem is an area of ongoing research. Here, we use the method described in [5] (see Appendix A.1 for more details).

2.2. Description of Data with Gaussian Noise

For the data generating mechanism, we assume that the observations arise when the solution to a system of the form (1) gets corrupted by noise. For simplicity, the data is assumed to be observed on a uniform grid with stepsize Δt . For the Gaussian case, we further assume that the noise is additive, consisting of independent and identically distributed (i.i.d.) Gaussian random variables. Specifically, for sample timepoints $\{t_m\}_{m=0}^M$, and true states $\mathbf{u}_m^* := \mathbf{u}(t_m)$, we assume that the observed data arise as a sum of the true state and noise:

$$\mathbf{u}_m = \mathbf{u}_m^* + \boldsymbol{\varepsilon}_m \quad \forall m \in \{0, \dots, M\}$$

where $\boldsymbol{\varepsilon}_m \stackrel{iid}{\sim} \mathcal{N}(\mathbf{0}, \boldsymbol{\Sigma})$, and $\boldsymbol{\Sigma}$ is a $D \times D$ diagonal matrix. In Section 2.6 we will adapt this framework to accommodate the multiplicative log-normal noise instead of Gaussian.

2.3. Discretization

For the set of test functions $\{\varphi_k\}_{k=1}^K$, we build the matrices

$$\boldsymbol{\Phi} = \begin{bmatrix} \varphi_1(\mathbf{t})^T \\ \vdots \\ \varphi_K(\mathbf{t})^T \end{bmatrix} \in \mathbb{R}^{K \times (M+1)}, \quad \dot{\boldsymbol{\Phi}} = \begin{bmatrix} \dot{\varphi}_1(\mathbf{t})^T \\ \vdots \\ \dot{\varphi}_K(\mathbf{t})^T \end{bmatrix} \in \mathbb{R}^{K \times (M+1)}$$

The matrices of the data and the RHS are as follows:

$$\mathbf{t} := \begin{bmatrix} t_0 \\ \vdots \\ t_M \end{bmatrix} \in \mathbb{R}^{(M+1) \times 1}, \quad \mathbf{U} := \begin{bmatrix} \mathbf{u}_0^T \\ \vdots \\ \mathbf{u}_M^T \end{bmatrix} \in \mathbb{R}^{(M+1) \times D}, \quad \mathbf{F}(\mathbf{p}; \mathbf{U}, \mathbf{t}) := \begin{bmatrix} \mathbf{f}(\mathbf{p}, \mathbf{u}_1, t_1)^T \\ \vdots \\ \mathbf{f}(\mathbf{p}, \mathbf{u}_M, t_M)^T \end{bmatrix} \in \mathbb{R}^{(M+1) \times D}.$$

‡ One could choose more general test functions $\varphi(t) = [\varphi_1(t), \dots, \varphi_D(t)]^T$ and the derivations here can be easily extended to this case.

The products $\dot{\Phi}\mathbf{U}$ and $\Phi\mathbf{F}$ are equivalent to using the trapezoid rule to numerically approximate the integral in the inner product \S . Therefore, the discretization of (3) is

$$-\dot{\Phi}\mathbf{U} \approx \Phi\mathbf{F}(\mathbf{p}; \mathbf{U}, \mathbf{t}) \quad (4)$$

and would be satisfied perfectly if there was no noise and no numerical error in the quadrature. This motivates inspecting the weak residual, which we define as:

$$\mathbf{r}(\mathbf{p}; \mathbf{U}, \mathbf{t}) = \mathbf{g}(\mathbf{p}; \mathbf{U}, \mathbf{t}) - \mathbf{b}(\mathbf{U}) \quad (5)$$

where

$$\mathbf{g}(\mathbf{p}; \mathbf{U}, \mathbf{t}) := \text{vec}[\Phi\mathbf{F}(\mathbf{p}; \mathbf{U}, \mathbf{t})], \quad \mathbf{b}(\mathbf{U}) := -\text{vec}[\dot{\Phi}\mathbf{U}]$$

and “vec” is the columnwise vectorization of a matrix. Since the noise $\epsilon_m \stackrel{iid}{\sim} N(\mathbf{0}, \Sigma)$, we know that $\text{vec}[\mathcal{E}] \sim N(\mathbf{0}, \Sigma \otimes \mathbb{I}_{M+1})$ where \otimes is the Kronecker product and $\mathbb{I}_{M+1} \in \mathbb{R}^{(M+1) \times (M+1)}$ is the identity matrix.

2.4. Distribution of the Weak Residual

The idea of using the weak form equation error residual has been used since the 1950’s for parameter estimation [58]. However, equation error-based estimation (both weak and strong form) exhibit a known bias [53]. When the system is LiP, the effect can be diminished via correcting the covariance using an accurate statistical model for the noise [5]. When the system is NiP, however, the residual \mathbf{r} is a nontrivial transform of the corrupted data.

In this section, we provide a theoretical derivation of the distribution of the residual via two propositions and a lemma, followed by several remarks on the consequences of this result.

Proposition 1. *Let uncorrupted data \mathbf{U}^* and true parameters \mathbf{p}^* satisfy Equation (2) on the time domain $[0, T]$. Assuming that \mathbf{f} is continuous in time, the following holds:*

$$\lim_{M \rightarrow \infty} \|\mathbf{r}^{\text{int}}\| = 0$$

where $\mathbf{r}^{\text{int}} = \mathbf{r}(\mathbf{p}^*; \mathbf{U}^*, \mathbf{t})$

Proof. The true data satisfies the weak form of the system of differential equations as stated in Equation (2) for all possible test functions. The k^{th} entry of \mathbf{r}^{int} is an approximation of Equation (2) for a particular test function φ_k :

$$r_k^{\text{int}} = \underbrace{\langle \varphi_k, \mathbf{f}(\mathbf{p}^*, \mathbf{u}, t) \rangle + \langle \dot{\varphi}_k, \mathbf{u} \rangle}_{=0} + \mathbf{e}^{\text{int}}$$

\S If the grid was non-uniform or if a different quadrature rule was desired, then the test function matrices would be post-multiplied by a quadrature matrix \mathcal{Q} . In the case of the trapezoid rule, that matrix is $\Delta t I$ except for the (1, 1) and $(M + 1, M + 1)$ entries which are $\Delta t/2$. However, the compact support of φ means that the $\Delta t/2$ values will be multiplied by a zero and thus we can disregard the whole matrix (see the discussion between Equations (5) and (6) on page 7 of [5]).

The inner products are computed via a quadrature rule. Relying on the assumption that $\mathbf{u}(t)$ is in a Sobolev space, for a fixed time domain the integration error, \mathbf{e}^{int} , converges to zero as the number of points M increases:

$$\lim_{M \rightarrow \infty} \|\mathbf{r}^{\text{int}}\| = \lim_{M \rightarrow \infty} \|\mathbf{e}^{\text{int}}\| = 0.$$

□

Proposition 2. For uncorrupted data \mathbf{U}^* and true parameters \mathbf{p}^* that satisfy Equation (2), we define the corrupted data as $\mathbf{U} = \mathbf{U}^* + \mathcal{E}$, where $\mathcal{E} \sim \mathcal{N}(\mathbf{0}, \Sigma \otimes \mathbb{I}_{M+1})$. Assuming that \mathbf{f} is twice continuously differentiable in \mathbf{u} , the following holds:

$$\mathbf{S}(\mathbf{p}^*; \mathbf{U}, \mathbf{t})^{-\frac{1}{2}} \mathbf{r}^{\text{lin}} \sim \mathcal{N}(\mathbf{0}, \mathbb{I}_{KD}) \text{ and } \mathbb{E}[\|\mathbf{r}^\varepsilon - \mathbf{r}^{\text{lin}}\|] = \mathcal{O}\left(\mathbb{E}[\|\text{vec}[\mathcal{E}]\|^2]\right)$$

where

$$\begin{aligned} \mathbf{r}^{\text{lin}} &:= \nabla_{\mathbf{u}} \mathbf{g}(\mathbf{p}^*; \mathbf{U}, \mathbf{t}) \text{vec}[\mathcal{E}] - \mathbf{b}(\mathcal{E}), \\ \mathbf{r}^\varepsilon &:= \mathbf{g}(\mathbf{p}^*; \mathbf{U}, \mathbf{t}) - \mathbf{g}(\mathbf{p}^*; \mathbf{U}^*, \mathbf{t}) - \mathbf{b}(\mathcal{E}), \end{aligned}$$

$$\mathbf{S}(\mathbf{p}^*; \mathbf{U}, \mathbf{t}) := \left(\nabla_{\mathbf{u}} \mathbf{g}(\mathbf{p}^*; \mathbf{U}, \mathbf{t}) + (\dot{\Phi} \otimes \mathbb{I}_D) \right) \left(\Sigma \otimes \mathbb{I}_{M+1} \right) \left((\nabla_{\mathbf{u}} \mathbf{g}(\mathbf{p}^*; \mathbf{U}, \mathbf{t}))^T + (\dot{\Phi}^T \otimes \mathbb{I}_D) \right),$$

and $\nabla_{\mathbf{u}} \mathbf{g}(\mathbf{p}^*; \mathbf{U}, \mathbf{t}) \in \mathbb{R}^{KD \times D(M+1)}$ is the Jacobian matrix of $\mathbf{g}(\mathbf{p}^*; \mathbf{U}, \mathbf{t})$ with respect to the state variable, \mathbf{u} .

Proof. First, the distribution of \mathbf{r}^{lin} follows from the Gaussian distribution of \mathcal{E} . Since the linear combination of Gaussians is also Gaussian, we can compute the following mean and covariance conditioned on the observed data:

$$\begin{aligned} \mathbb{E}[\mathbf{r}^{\text{lin}} \mid \mathbf{U}] &= 0 \\ \mathbb{E}[\mathbf{r}^{\text{lin}} (\mathbf{r}^{\text{lin}})^T \mid \mathbf{U}] &= \left(\nabla_{\mathbf{u}} \mathbf{g}(\mathbf{p}^*; \mathbf{U}, \mathbf{t}) + (\dot{\Phi} \otimes \mathbb{I}_D) \right) \left(\Sigma \otimes \mathbb{I}_{M+1} \right) \left((\nabla_{\mathbf{u}} \mathbf{g}(\mathbf{p}^*; \mathbf{U}, \mathbf{t}))^T + (\dot{\Phi}^T \otimes \mathbb{I}_D) \right). \end{aligned}$$

To obtain the expected error from \mathbf{r}^{lin} to \mathbf{r}^ε , we begin by expanding \mathbf{r}^ε about the data \mathbf{U} . Taylor's Remainder Theorem guarantees that $\exists \hat{\mathbf{U}} \in \{X \in \mathbb{R}^{(M+1) \times D} \mid \|X - U\|_\infty \leq \|\mathbf{U} - \mathbf{U}^*\|_\infty\}$ such that

$$\mathbf{r}^\varepsilon = \mathbf{g}(\mathbf{p}^*; \mathbf{U}, \mathbf{t}) - \mathbf{b}(\mathcal{E}) - (\mathbf{g}(\mathbf{p}^*; \mathbf{U}, \mathbf{t}) - \nabla_{\mathbf{u}} \mathbf{g}(\mathbf{p}^*; \mathbf{U}, \mathbf{t}) \text{vec}[\mathcal{E}] + (\mathbf{H}_{\mathbf{u}}(\mathbf{g})(\mathbf{p}^*; \hat{\mathbf{U}}, \mathbf{t}) \bar{\times}_3 \text{vec}[\mathcal{E}]) \bar{\times}_2 \text{vec}[\mathcal{E}])$$

where $\mathbf{H}_{\mathbf{u}}(\mathbf{g}) : \mathbb{R}^J \times \mathbb{R}^{(M+1) \times D} \times \mathbb{R}^{M+1} \rightarrow \mathbb{R}^{KD \times (M+1)D \times (M+1)D}$ is the Hessian of \mathbf{g} with respect to \mathbf{u} . The $\mathbf{g}(\mathbf{p}^*; \mathbf{U}, \mathbf{t})$ terms cancel

$$\mathbf{r}^\varepsilon = \underbrace{\nabla_{\mathbf{u}} \mathbf{g}(\mathbf{p}^*; \mathbf{U}, \mathbf{t}) \text{vec}[\mathcal{E}] - \mathbf{b}(\mathcal{E})}_{=\mathbf{r}^{\text{lin}}} + (\mathbf{H}_{\mathbf{u}}(\mathbf{g})(\mathbf{p}^*; \hat{\mathbf{U}}, \mathbf{t}) \bar{\times}_3 \text{vec}[\mathcal{E}]) \bar{\times}_2 \text{vec}[\mathcal{E}].$$

Subtracting \mathbf{r}^{lin} , taking the expectation of the norm of both sides, and then applying triangle inequality simplifies to the desired result

$$\mathbb{E}[\|\mathbf{r}^\varepsilon - \mathbf{r}^{\text{lin}}\|] = \mathcal{O}\left(\mathbb{E}[\|\text{vec}[\mathcal{E}]\|^2]\right).$$

□

|| Here $\bar{\times}_n$ specifies the n -mode (vector) product of a tensor with a vector (see section 2.5 of [27]).

Lemma 1. *Let true data \mathbf{U}^* and true parameters \mathbf{p}^* satisfy Equation (2) on the time domain $[0, T]$, and for noise $\text{vec}[\mathcal{E}] \sim \mathcal{N}(\mathbf{0}, \boldsymbol{\Sigma} \otimes \mathbb{I}_{M+1})$, and corrupted data $\mathbf{U} = \mathbf{U}^* + \mathcal{E}$. Assuming that \mathbf{f} is continuous in t and twice continuously differentiable in \mathbf{u} , the following holds:*

$$\mathbf{S}(\mathbf{p}^*; \mathbf{U}, \mathbf{t})^{-\frac{1}{2}} \mathbf{r}^{\text{lin}}(\mathbf{p}^*; \mathbf{U}, \mathbf{t}) \sim \mathcal{N}(\mathbf{0}, \mathbb{I}_{KD}) \text{ and } \lim_{M \rightarrow \infty} \mathbb{E} \left[\|\mathbf{r} - \mathbf{r}^{\text{lin}}\| \right] = \mathcal{O} \left(\mathbb{E} [\|\text{vec}[\mathcal{E}]\|^2] \right)$$

Proof. This derivation is a natural extension of the one in [5]. The key difference is that now it is not assumed that \mathbf{F} is linear in \mathbf{p} , and \mathbf{F} can explicitly depend on t .

Regardless of the form of \mathbf{f} , we have that \mathbf{b} is linear, thus:

$$\mathbf{b}(\mathbf{U}) = \mathbf{b}(\mathbf{U}^*) + \mathbf{b}(\mathcal{E})$$

Now consider \mathbf{p}^* to be the true parameters.

$$\mathbf{r}(\mathbf{p}^*; \mathbf{U}, \mathbf{t}) = \mathbf{g}(\mathbf{p}^*; \mathbf{U}, \mathbf{t}) - \mathbf{g}(\mathbf{p}^*; \mathbf{U}^*, \mathbf{t}) + \mathbf{g}(\mathbf{p}^*; \mathbf{U}^*, \mathbf{t}) - \mathbf{b}(\mathbf{U}^*) - \mathbf{b}(\mathcal{E})$$

Regrouping terms isolates the sources of error in the weak residual:

$$\begin{aligned} \mathbf{r}(\mathbf{p}^*; \mathbf{U}, \mathbf{t}) &= \underbrace{\mathbf{g}(\mathbf{p}^*; \mathbf{U}^*, \mathbf{t}) - \mathbf{b}(\mathbf{U}^*)}_{=\mathbf{r}^{\text{int}}} + \underbrace{\mathbf{g}(\mathbf{p}^*; \mathbf{U}, \mathbf{t}) - \mathbf{g}(\mathbf{p}^*; \mathbf{U}^*, \mathbf{t}) - \mathbf{b}(\mathcal{E})}_{=\mathbf{r}^{\text{e}}} \\ \lim_{M \rightarrow \infty} \mathbb{E} \left(\|\mathbf{r} - \mathbf{r}^{\text{lin}}\| \right) &\leq \lim_{M \rightarrow \infty} \mathbb{E} \left(\|\mathbf{r}^{\text{int}}\| \right) + \mathbb{E} \left(\|\mathbf{r}^{\text{e}} - \mathbf{r}^{\text{lin}}\| \right) \end{aligned}$$

Combining the results from Propositions 1 and 2, the result holds. \square

Remark 1 (Spectral Convergence of Integration Error). *The grid is assumed to be uniform, so the quadrature rule chosen is the trapezoidal rule. This quadrature rule has spectral convergence because the periodic extension of a compact functions is itself [3]. In particular, the order of the numerical error is $\mathcal{O}(\Delta t)^{(p+1)}$ where p is the order of the smoothness of the test function at the endpoints of the integral domain. Thus in this context, \mathbf{r}^{int} is negligible due the smoothness of $\varphi * u$.*

Remark 2 (Higher Order Terms). *Unfortunately, higher order terms may not be negligible in noise regimes of interest, making the likelihood from the distribution in Lemma 1 unrepresentative of the true likelihood of the weak residual. In practice, the Gaussian approximation still leads to reasonable estimates of the parameters, especially when \mathbf{f} has less nonlinearity with respect to \mathbf{u} and at lower noise levels.*

2.5. Weak Likelihood Function

In the previous WENDy-IRLS work [5], the covariance information was leveraged by applying an Iteratively Reweighted Least Squares (WENDy-IRLS) algorithm as described in Appendix C. Experimentally, we found that WENDy-IRLS did not converge sometimes when differential systems were highly nonlinear in the state variable \mathbf{u} and when noise levels became too high. To prevent that, we now consider optimizing the

negative log-likelihood of the weak residual to approximate the MLE. Because the residual has a conditional distribution that is multivariate normal, we can explicitly write down the analytic form of this weak negative log-likelihood:

$$\begin{aligned} \ell(\mathbf{p}; \mathbf{U}, \mathbf{t}) &= \frac{1}{2} (KD \log(2\pi) + \log(\det(\mathbf{S}(\mathbf{p}; \mathbf{U}, \mathbf{t}))) \\ &\quad + (\mathbf{g}(\mathbf{p}; \mathbf{U}, \mathbf{t}) - \mathbf{b}(\mathbf{U}))^T \mathbf{S}(\mathbf{p}; \mathbf{U}, \mathbf{t})^{-1} (\mathbf{g}(\mathbf{p}; \mathbf{U}, \mathbf{t}) - \mathbf{b}(\mathbf{U}))). \end{aligned} \quad (6)$$

Notice that ℓ is the sum of three terms. The first, $KD \log(2\pi)$, is constant with respect to \mathbf{p} , and thus can be neglected in optimization. The second, $\log(\det(\mathbf{S}(\mathbf{p}; \mathbf{U}, \mathbf{t})))$, only depends on the eigenvalues of the covariance, and penalizes parameter values that lead to large uncertainty. The third term is the Mahalanobis Distance which is the Euclidean norm weighted by the covariance matrix, and penalizes parameter values that lead to large residuals. Balancing these last two terms minimizes uncertainty and equation error. Because the analytic form of the likelihood is known and can be efficiently computed, we can make use of modern optimization algorithms to find the MLE.

2.5.1. Derivative Information First and second order derivative information of ℓ can be derived analytically, allowing for efficient use of second-order optimization routines that are robust to non-convex problems. All the derivative computations assume \mathbf{f} is twice continuously differentiable in \mathbf{p} . For ease of notation and because the data is fixed, we drop explicit dependence on \mathbf{U} and \mathbf{t} : $\ell(\mathbf{p}) := \ell(\mathbf{p}; \mathbf{U}, \mathbf{t})$, $\mathbf{S}(\mathbf{p}) := \mathbf{S}(\mathbf{p}; \mathbf{U}, \mathbf{t})$, $\mathbf{g}(\mathbf{p}) := \mathbf{g}(\mathbf{p}; \mathbf{U}, \mathbf{t})$, and $\mathbf{b} := \mathbf{b}(\mathbf{U})$.

Gradient Information Regardless of the linearity of \mathbf{f} with respect to \mathbf{p} , the j^{th} component of the gradient of the weak log-likelihood is given as

$$\begin{aligned} \partial_{\mathbf{p}_j} \ell(\mathbf{p}) &= \frac{1}{2} \left(\text{Tr}(\mathbf{S}(\mathbf{p})^{-1} \partial_{\mathbf{p}_j} \mathbf{S}(\mathbf{p})) \right. \\ &\quad \left. + 2(\partial_{\mathbf{p}_j} \mathbf{g}(\mathbf{p}))^T \mathbf{S}(\mathbf{p})^{-1} (\mathbf{g}(\mathbf{p}) - \mathbf{b}) \right. \\ &\quad \left. + (\mathbf{g}(\mathbf{p}) - \mathbf{b})^T (\partial_{\mathbf{p}_j} \mathbf{S}(\mathbf{p})^{-1}) (\mathbf{g}(\mathbf{p}) - \mathbf{b}) \right) \end{aligned} \quad (7)$$

where

$$\begin{aligned} \partial_{\mathbf{p}_j} \mathbf{S}(\mathbf{p})^{-1} &= -\mathbf{S}(\mathbf{p})^{-1} (\partial_{\mathbf{p}_j} \mathbf{S}(\mathbf{p})) \mathbf{S}(\mathbf{p})^{-1} \\ \partial_{\mathbf{p}_j} \mathbf{S}(\mathbf{p}) &= \partial_{\mathbf{p}_j} \nabla_{\mathbf{u}} \mathbf{g}(\mathbf{p}) (\boldsymbol{\Sigma} \otimes \mathbb{I}_{M+1}) (\nabla_{\mathbf{u}} \mathbf{g}(\mathbf{p}) + \dot{\boldsymbol{\Phi}} \otimes \mathbb{I}_D)^T. \end{aligned}$$

Hessian Information Taking derivatives again, the elements of Hessian are

$$\begin{aligned} \partial_{\mathbf{p}_i, \mathbf{p}_j} \ell(\mathbf{p}) &= \frac{1}{2} \left(\text{Tr}(\partial_{\mathbf{p}_i} \mathbf{S}(\mathbf{p})^{-1} \partial_{\mathbf{p}_j} \mathbf{S}(\mathbf{p}) + \mathbf{S}(\mathbf{p})^{-1} \partial_{\mathbf{p}_i, \mathbf{p}_j} \mathbf{S}(\mathbf{p})) \right. \\ &\quad \left. + 2(\partial_{\mathbf{p}_j} \mathbf{g}(\mathbf{p}))^T (\partial_{\mathbf{p}_i} \mathbf{S}(\mathbf{p})^{-1}) (\mathbf{g}(\mathbf{p}) - \mathbf{b}) \right. \\ &\quad \left. + 2(\partial_{\mathbf{p}_j} \mathbf{g}(\mathbf{p}))^T \mathbf{S}(\mathbf{p})^{-1} \partial_{\mathbf{p}_i} \mathbf{g}(\mathbf{p}) \right. \\ &\quad \left. + 2(\partial_{\mathbf{p}_i, \mathbf{p}_j} \mathbf{g}(\mathbf{p}))^T \mathbf{S}(\mathbf{p})^{-1} (\mathbf{g}(\mathbf{p}) - \mathbf{b}) \right. \\ &\quad \left. + (\mathbf{g}(\mathbf{p}) - \mathbf{b})^T (\partial_{\mathbf{p}_i, \mathbf{p}_j} \mathbf{S}(\mathbf{p})^{-1}) (\mathbf{g}(\mathbf{p}) - \mathbf{b}) \right) \end{aligned} \quad (8)$$

where

$$\begin{aligned}\partial_{\mathbf{p}_i \mathbf{p}_j} \mathbf{S}(\mathbf{p})^{-1} &= \mathbf{S}(\mathbf{p})^{-1} \partial_{\mathbf{p}_i} \mathbf{S}(\mathbf{p}) \mathbf{S}(\mathbf{p})^{-1} \partial_{\mathbf{p}_j} \mathbf{S}(\mathbf{p}) \mathbf{S}(\mathbf{p})^{-1} \\ &\quad - \mathbf{S}(\mathbf{p})^{-1} \partial_{ij} \mathbf{S}(\mathbf{p}) \mathbf{S}(\mathbf{p})^{-1} \\ &\quad + \mathbf{S}(\mathbf{p})^{-1} \partial_{\mathbf{p}_j} \mathbf{S}(\mathbf{p}) \mathbf{S}(\mathbf{p})^{-1} \partial_{\mathbf{p}_i} \mathbf{S}(\mathbf{p}) \mathbf{S}(\mathbf{p})^{-1} \\ \partial_{\mathbf{p}_i \mathbf{p}_j} \mathbf{S}(\mathbf{p}) &= (\partial_{\mathbf{p}_i \mathbf{p}_j} \nabla_{\mathbf{u}} \mathbf{g}(\mathbf{p})) (\boldsymbol{\Sigma} \otimes \mathbb{I}_{M+1}) (\nabla_{\mathbf{u}} \mathbf{g}(\mathbf{p}) + \dot{\Phi} \otimes \mathbb{I}_D)^T \\ &\quad + (\partial_{\mathbf{p}_j} \nabla_{\mathbf{u}} \mathbf{g}(\mathbf{p})) (\boldsymbol{\Sigma} \otimes \mathbb{I}_{M+1}) (\partial_{\mathbf{p}_i} \mathbf{g}(\mathbf{p}))^T.\end{aligned}$$

2.6. Extending to Log-Normal Noise

In many systems, it is more appropriate to have multiplicative log-normal noise rather than additive Gaussian noise. This is particularly true when the state variable cannot be negative. This formally means the data is corrupted in the following way

$$\mathbf{u}_m = \mathbf{u}_m^* \circ \boldsymbol{\nu}_m \quad \forall m \in \{0, \dots, M\}$$

where $\log(\boldsymbol{\nu}_m) \stackrel{\text{iid}}{\sim} N(\mathbf{0}, \boldsymbol{\Sigma})$ and \circ denotes the Hadamard Product meaning multiplication occurs element-wise. Our convention is that logarithms and exponentials are applied element-wise.

The result from Lemma 1 can be extended to the log-normal case.

Corollary 1. *Let true data \mathbf{U}^* and true parameters \mathbf{p}^* satisfy Equation (2) on the time domain $[0, T]$, and for noise $\log(\mathcal{V}) \sim N(\mathbf{0}, \boldsymbol{\Sigma} \otimes \mathbb{I}_{M+1})$, and corrupted data $\mathbf{U} = \mathbf{U}^* \circ \mathcal{V}$. Assuming the $\tilde{\mathbf{f}}$ is continuous in t and twice continuously differentiable in \mathbf{u} , the following holds for transformed weak residual:*

$$\tilde{\mathbf{S}}(\mathbf{p}^*, \mathbf{U}, \mathbf{t})^{-\frac{1}{2}} \tilde{\mathbf{r}}^{\text{lin}}(\mathbf{p}^*; \mathbf{U}, \mathbf{t}) \sim N(\mathbf{0}, \mathbb{I}_{KD}) \text{ and } \mathbb{E}[\|\tilde{\mathbf{r}} - \tilde{\mathbf{r}}^{\text{lin}}\|] = \mathcal{O}\left(\mathbb{E}[\|\text{vec}[\log(\mathcal{V})]\|^2]\right)$$

where \oslash is element-wise division and

$$\tilde{\mathbf{f}}(\mathbf{p}, \mathbf{U}, \mathbf{t}) := \mathbf{f}(\mathbf{p}, \mathbf{u}, t) \oslash \mathbf{u}, \quad \tilde{\mathbf{g}}(\mathbf{p}; \mathbf{U}, \mathbf{t}) := \text{vec}[\Phi \tilde{\mathbf{f}}(\mathbf{p}, \mathbf{U}, \mathbf{t})]$$

$$\tilde{\mathbf{b}}(\mathbf{U}) := \text{vec}[-\dot{\Phi} \log(\mathbf{U})], \quad \tilde{\mathbf{r}} := \tilde{\mathbf{g}}(\mathbf{p}; \mathbf{U}, \mathbf{t}) - \tilde{\mathbf{b}}(\mathbf{U}), \quad \tilde{\mathbf{r}}^{\text{lin}} := \nabla_{\mathbf{u}} \tilde{\mathbf{g}}(\mathbf{p}^*; \mathbf{U}, \mathbf{t}) \text{vec}[\log(\mathcal{V})] - \tilde{\mathbf{b}}(\mathcal{V}),$$

$$\tilde{\mathbf{S}}(\mathbf{p}; \mathbf{U}, \mathbf{t}) := (\nabla_{\log(\mathbf{u})} \tilde{\mathbf{g}}(\mathbf{p}; \mathbf{U}, \mathbf{t}) + \dot{\Phi}) (\boldsymbol{\Sigma} \otimes \mathbb{I}_{M+1}) (\nabla_{\log(\mathbf{u})} \tilde{\mathbf{g}}(\mathbf{p}; \mathbf{U}, \mathbf{t}) + \dot{\Phi})^T$$

Proof. Start by defining a change of variables:

$$\{\mathbf{x}_m\}_{m=0}^M := \{\log(\mathbf{u}_m)\}_{m=0}^M = \{\log(\mathbf{u}_m^*) + \log(\boldsymbol{\nu}_m)\}_{m=0}^M.$$

We build the corresponding data matrix $\mathbf{X} := [\mathbf{x}_0 \quad \dots \quad \mathbf{x}_M]$. Applying chain rule we see that \mathbf{x} satisfies the following ODE:

$$\frac{d\mathbf{x}}{dt} = \mathbf{f}(\mathbf{p}, \exp(\mathbf{x}), t) \oslash \exp(\mathbf{x})$$

Thus, we have the corresponding weak form of the ODE for transformed state variable:

$$-\langle \dot{\varphi}, \mathbf{x} \rangle = \langle \varphi, \mathbf{f}(\mathbf{p}, \exp(\mathbf{x}), t) \oslash \exp(\mathbf{x}) \rangle.$$

Notice that for \mathbf{X} , the noise is now additive and Gaussian, thus we satisfy the assumptions of Lemma 1, and can obtain the desired result. \square

Remark 3 (Derivative Computations for the Log-Normal Case). *In practice, the computations for the RHS, LHS and corresponding derivatives stay identically the same, modulo the replacing of \mathbf{b} with $\tilde{\mathbf{b}}$ and \mathbf{f} with $\tilde{\mathbf{f}}$. The computations for $\partial_{\mathbf{p}_j} \nabla_{\mathbf{u}} \mathbf{g}(\mathbf{p}; \mathbf{U}, \mathbf{t})$ and $\partial_{\mathbf{p}_i, \mathbf{p}_j} \nabla_{\mathbf{u}} \mathbf{g}(\mathbf{p}; \mathbf{U}, \mathbf{t})$ now become $\partial_{\mathbf{p}_j} \nabla_{\mathbf{x}} \mathbf{g}(\mathbf{p}; \exp(\mathbf{X}))$ and $\partial_{\mathbf{p}_i, \mathbf{p}_j} \nabla_{\mathbf{x}} \mathbf{g}(\mathbf{p}; \exp(\mathbf{X}))$, respectively.*

2.7. Distribution of Parameter Estimator

Relying on the asymptotic consistency of the MLE, $\hat{\mathbf{p}} \xrightarrow{P} \mathbf{p}^*$, the uncertainty information of the parameters can be estimated from the result of the WENDy-MLE algorithm. When the dynamics are nonlinear, we again utilize a linearization of \mathbf{g} , but this time with respect to \mathbf{p} . This procedure works when the map, $\mathbf{r}(\mathbf{p})$, is surjective. Empirically, this is true in practice because the Jacobian happens to be full rank. We can derive an approximation to the distribution of the estimator as follows:

$$\left((\nabla_{\mathbf{p}} \mathbf{g})^+ \mathbf{S}(\mathbf{p}^*) (\nabla_{\mathbf{p}} \mathbf{g})^+ \right)^{-\frac{1}{2}} \mathbf{p} \overset{approx}{\sim} \mathcal{N}(\mathbf{p}^*, \mathbb{I}_J) \quad (9)$$

where $(\nabla_{\mathbf{p}} \mathbf{g})^+$ is the Moore–Penrose inverse of $\nabla_{\mathbf{p}} \mathbf{g}$. The approximation becomes more accurate as $M \rightarrow \infty$. This provides powerful information about WENDy-MLE estimated parameters; the algorithm is able to provide both an estimate and the uncertainty information about the estimate.

3. Implementation and Numerical Results

This section contains a description of the maximum likelihood WENDy-MLE algorithm as well as the numerical results. In Section 3.1 we will discuss the algorithmic implementation. Then we introduce the details of a forward solver method used for comparison in Section 3.2. Next, the details of the metrics are shown in Section 3.3, and artificial noise is discussed in Section 3.4. Our results begin in Section 3.5 where a motivating example demonstrates why alternatives to forward simulation based methods are necessary. Finally in Section 3.6, results for a suite of test problems demonstrate key capabilities of the WENDy-MLE algorithm.

3.1. WENDy-MLE Algorithm

By explicitly forming the likelihood function for the weak residual in Equation (6) and its derivative in Equations (7) and (8), estimating the parameters can be framed as the following optimization problem:

$$\hat{\mathbf{p}} = \underset{\substack{\mathbf{p} \in \mathbb{R}^J \\ \mathbf{p}_\ell \leq \mathbf{p} \leq \mathbf{p}_u}}{\operatorname{argmin}} \ell(\mathbf{p}) \quad (10)$$

In general, this is a non-convex optimization problem, so it is appropriate to use trust-region second order methods that have been developed for this purpose.

WENDy-MLE takes the time grid \mathbf{t} , data \mathbf{U} , a function for the RHS, \mathbf{f} , an initial guess for the parameters \mathbf{p}_0 , and optionally box constraints for the parameters, \mathbf{p}_ℓ and \mathbf{p}_u . For most of the examples explored here, the unconstrained and constrained optimizers return nearly identical results.

`Symbolics.jl` [17] is used to compute all partial derivative of \mathbf{f} , and then Julia functions are formed from those symbolic expression. Then, the weak likelihood and its derivatives can be evaluated using Equations (6), (7), and (8). These functions are then used in second order optimization methods¶. Trust region solvers are provided by `JSOSolvers.jl` and `Optim.jl` for the constrained and unconstrained cases respectively [25, 43]. We note that our code also supports using the Adaptive Regularization Cubics variant (ARCqK) in the unconstrained case provide by `AdaptiveRegularization.jl` [13]. The trust region solvers and ARCqK usually produce similar results, but in our limited testing we found the trust region solvers work better in general, so only results for the trust region solver are shown. Our code, `WENDy.jl`, is readily available through the Julia package manager.

3.2. Output Error Solver

For comparison, we use the standard output error approach of regressing the approximated state against the data. This is done by iteratively calling a direct numerical forward solver and optimizing over both the initial condition and the unknown parameters. We include the initial conditions as an optimization parameter since otherwise noisy initial data can drastically effect output error depending on the sensitivity of the system. The full scheme can be framed as a nonlinear least squares problem:

$$\hat{\mathbf{p}} = \operatorname{argmin}_{\mathbf{p} \in \mathbb{R}^J} \left[\min_{\mathbf{u}_0 \in \mathbb{R}^D} \frac{1}{2} \left\| \hat{\mathbf{U}}(\mathbf{p}, \mathbf{u}_0) - \mathbf{U} \right\|_F^2 \right]. \quad (11)$$

We refer to this method Output Error Least Squares (OE-LS). Forward simulation is accomplished with the Rodas4P algorithm provided by `DifferentialEquations.jl` [51]. This solver is well suited to solve stiff system, so it is appropriate for all the example problems discussed here. Nonlinear least squares problems are solved by the Levenberg-Marquardt algorithm through `NonlinearSolve.jl` [45]. Derivative information is computed via automatic differentiation provided by `ForwardDiff.jl` [54].

3.3. Metrics

Depending on the motivation behind the system identification, one may either care about identifying the parameters themselves, or only care about predictive performance. Hence

¶ While the likelihood is a scalar valued function, its computation relies on the derivatives of vector and matrix valued functions. Building and using efficient data structures to compute these derivative can rely on “vectorization” resulting large matrices with block structure from Kronecker products. In our implementation we instead use multidimensional arrays and define the operations in Einstein summation notation. These computations are then evaluated efficiently with `Tullio.jl` [1].

Metric	Formula
Relative Coefficient Error	$\frac{\ \hat{\mathbf{p}} - \mathbf{p}^*\ _2}{\ \mathbf{p}^*\ _2} \quad (12)$
Mean Forward Simulation Relative Error	$\frac{\ \hat{\mathbf{U}}(\mathbf{p}, \mathbf{u}_0) - \mathbf{U}^*\ _F}{\ \mathbf{U}^*\ _F} \quad (13)$
Failure Rate	$\frac{1}{N} \sum_{n=1}^N \chi_F(\hat{\mathbf{p}}^{(n)})$ $F = \{\mathbf{p} \mid \text{forward simulation fails}\} \quad (14)$
Estimated Relative Squared Bias	$\frac{\left(\sum_{n=1}^N (\hat{p}_j^{(n)} - p_j^*)\right)^2}{N^2 (p_j^*)^2} \quad (15)$
Estimated Relative Variance	$\frac{\sum_{n=1}^N (\hat{p}_j^{(n)} - \bar{\hat{p}}_j)^2}{N (p_j^*)^2} \quad (16)$
Estimated Relative Mean Squared Error (MSE)	$\frac{\sum_{n=1}^N (\hat{p}_j^{(n)} - p_j^*)^2}{N (p_j^*)^2} \quad (17)$
Estimated Coverage	$\frac{1}{N} \sum_{n=1}^N \chi_A(\hat{p}_j^{(n)})$ $A = \left\{ \hat{p}_j \mid \hat{p}_j^{(n)} - p_j^* < 2\sqrt{C_{j,j}^{(n)}} \right\} \quad (18)$

Table 1: Notice, that in the computation for Mean Forward Simulation Relative Error the true initial condition is used. The metrics of bias, variance and mean squared error are averaged over all N runs. χ is the indicator function.

we look at two complementary metrics: Coefficient Relative Error and Mean Forward Solve Relative Error. When relevant we also report the failure rate. Furthermore, we provide statistical metrics for our estimator, including Estimated Relative Bias, Estimated Relative Variance, Estimated Relative Mean Square Error, and Coverage. All metrics are defined in Table 1.

We say an algorithm failed if its estimated parameters cause forward simulation to return NaN values. Failure rates are only reported when at least on algorithm failed more than 1% of the time. For failed runs their accuracy metrics are replaced with the

accuracy metric of the initial parameters, $\hat{\mathbf{p}}_0$.

3.4. Corrupting the Data With Artificial Noise

For testing purposes, the data is corrupted with noise before it is passed as an input to the WENDy-MLE or OE-LS algorithms. When noise is additive Gaussian, we add noise proportional to the size the state variables as described in Equation (19):

$$\begin{aligned} \boldsymbol{\varepsilon} &\stackrel{iid}{\sim} \mathcal{N}(0, \Sigma_{nr}) \\ \Sigma &= \text{diag} \left(\frac{\sigma_{nr} \|U\|_F^2}{M+1} \mathbf{1}_D \right) \end{aligned} \quad (19)$$

where σ_{nr} is the noise ratio. For the multiplicative log-normal noise we use a scale matrix of $\sigma_{nr} \mathbb{I}_D$:

$$\log(\boldsymbol{\nu}) \stackrel{iid}{\sim} \mathcal{N}(0, \sigma_{nr} \mathbb{I}_D). \quad (20)$$

3.5. Motivating Example: Lorenz Oscillator

The Lorenz Oscillator described by Equation (23) is a prototypical example of a chaotic system [61]. Estimating the parameters in a chaotic system is difficult with output error methods because forward simulation is sensitive to the initial conditions given. In practice true (noiseless) initial conditions are not always available. The weak form methods do not suffer from this complication in the same way.

To demonstrate this, we design an experiment where both solvers are given progressively more data from $[0, T]$ where $T \in \{3n\}_{n=1}^{10}$. One would hope that given more data, each algorithm would give progressively better estimates of the parameters, but in fact Figure 1 shows that in fact it gets worse with more data.

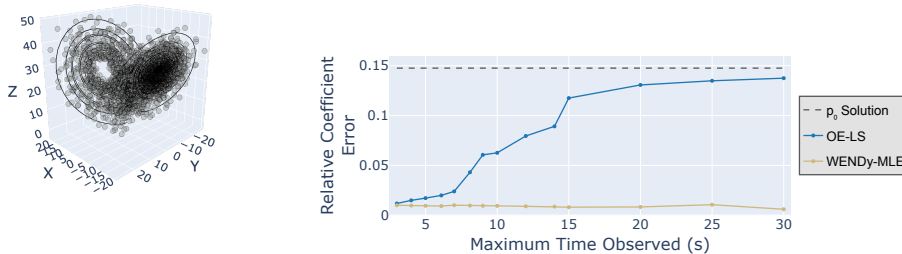


Figure 1: Left: the solution for the Lorenz oscillator in black and the corrupted data in grey dots. Right: the relative coefficient error for both the WENDy-MLE solver and the output error solver.

For this experiment, we run each algorithm thirty times for each T . On each run, we vary additive Gaussian noise and initial guess for the parameters. Noise is added

at a noise ratio of 10% as described in Equation (19). The data is given on a uniform grid with $\Delta T = 0.01$. The plot shows the mean coefficient relative error as described in Equation (12) for both algorithms as well as the initial parameters. As more data becomes available, WENDy-MLE maintains an excellent estimate of the parameters while the OE-LS estimate degrades monotonically.

3.6. Test Suite

We run both the WENDy-MLE and OE-LS algorithm over a suite of systems of differential equations described in Table 2. For each system, we run the algorithm 100 times at varying noise ratios and subsamplings of the data. Higher levels of noise and fewer data points increases the difficulty of recovering the unknown parameters. The final time is fixed at the specified value of T , but subsampling causes ΔT to increase.

Name	ODE	Parameters	Initial Parameterization
Logistic Growth	$\dot{u} = p_1 u + p_2 u^2$ (21)	$t \in [0, 10]$ $\mathbf{u}(0) = 0.01$ $\mathbf{p}^* = [1, -1]^T$	$p_1 \in [0, 10], p_2 \in [0, 10]$
Hindmarsh-Rose	$\begin{aligned} \dot{u}_1 &= p_1 u_2 - p_2 u_1^3 \\ &+ p_3 u_1^2 - p_4 u_3 \\ \dot{u}_2 &= p_5 - p_6 u_1^2 + p_7 u_2 \\ \dot{u}_3 &= p_8 u_1 + p_9 - p_{10} u_3 \end{aligned}$ (22)	$t \in [0, 10]$ $\mathbf{u}(0) = [-1.31, -7.6, -0.2]^T$ $\mathbf{p}^* = [10, 10, 30, 10, 10, 50, 10, 0.04, 0.0319, 0.01]^T$	$p_1 \in [0, 20], p_2 \in [0, 20]$ $p_3 \in [0, 60], p_4 \in [0, 20]$ $p_5 \in [0, 20], p_6 \in [0, 100]$ $p_7 \in [0, 20], p_8 \in [0, 1]$ $p_9 \in [0, 1], p_{10} \in [0, 1]$
Lorenz	$\begin{aligned} \dot{u}_1 &= p_1(u_2 - u_1) \\ \dot{u}_2 &= u_1(p_2 - u_3) - u_2 \\ \dot{u}_3 &= u_1 u_2 - p_3 u_3 \end{aligned}$ (23)	$t \in [0, 10]$ $\mathbf{u}(0) = [2, 1, 1]^T$ $\mathbf{p}^* = [10, 28, 8/3]^T$	$p_1 \in [0, 20], p_2 \in [0, 35]$ $p_3 \in [0, 5]$
Goodwin (2D)	$\begin{aligned} \dot{u}_1 &= \frac{p_1}{36 + p_2 u_2} - p_3 \\ \dot{u}_2 &= p_4 u_1 - p_5 \end{aligned}$ (24)	$t \in [0, 60]$ $\mathbf{u}(0) = [7, -10]^T$ $\mathbf{p}^* = [72, 1, 2, 1, 1]^T$	$p_1 \in [60, 80], p_2 \in [1, 3]$ $p_3 \in [0.5, 3], p_4 \in [0.5, 3]$ $p_5 \in [0.5, 3]$
Goodwin (3D)	$\begin{aligned} \dot{u}_1 &= \frac{p_1}{2.15 + p_3 u_3^4} - p_2 u_1 \\ \dot{u}_2 &= p_5 u_1 - p_6 u_2 \\ \dot{u}_3 &= p_7 u_2 - p_8 u_3 \end{aligned}$ (25)	$t \in [0, 80]$ $\mathbf{u}(0) = [0.3617, 0.9137, 1.3934]^T$ $\mathbf{p}^* = [3.4884, 0.0969, 10, 0.0969, 0.0581, 0.0969, 0.0775]^T$	$p_1 \in [1, 5], p_2 \in [0, 0.2]$ $p_3 \in [0, 2], p_4 \in [5, 15]$ $p_5 \in [0, 0.2], p_6 \in [0, 0.2]$ $p_7 \in [0, 0.2], p_8 \in [0, 0.2]$
SIR-TDI	$\begin{aligned} \dot{u}_1 &= -p_1 u_1 + p_3 u_2 \\ &+ \frac{p_1 e^{-p_1 p_2}}{1 - e^{-p_1 p_2}} u_3 \\ \dot{u}_2 &= p_1 u_1 - p_3 u_2 \\ &- p_4 (1 - e^{-p_5 t^2}) u_2 \\ \dot{u}_3 &= p_4 (1 - e^{-p_5 t^2}) u_2 \\ &- \frac{p_1 e^{-p_1 p_2}}{1 - e^{-p_1 p_2}} u_3 \end{aligned}$ (26)	$t \in [0, 50]$ $\mathbf{u}(0) = [1, 0, 0]^T$ $\mathbf{p}^* = [1.99, 1.5, 0.074, 0.113, 0.0024]^T$	$p_1 \in [10^{-4}, 1], p_2 \in [10^{-4}, 2]$ $p_3 \in [10^{-4}, 1], p_4 \in [10^{-4}, 1]$ $p_5 \in [10^{-4}, 1]$

Table 2: Table of example systems that are presented in the results.

Logistic Growth and Hindmarsh Rose are both linear in parameters and results were presented in the prior work of [5]. The improved WENDy-MLE algorithm presented here slightly improves accuracy metrics on these examples and adds significant robustness in the case of the Hindmarsh Rose. The Lorenz system is selected because it exemplifies why choosing a weak form method can be necessary. This system is affine in parameters but not linear. Both Goodwin models are chosen because they are NiP and have Hill functions that are of particular interest in many applications [21, 16]. The SIR-TDI model is NiP and was chosen to demonstrate WENDy-MLE's new ability to handle \mathbf{f}

with a direct dependence on t . Summary information about each system is shown in Table 3.

Name	Linear in Parameters	Noise Distribution
Logistic Growth	Linear	Additive normal
Hindmarsh-Rose	Linear	Additive normal
Lorenz	Linear	Additive normal
Goodwin (2D)	Nonlinear	Additive normal
Goodwin (3D)	Nonlinear	Multiplicative log-normal
SIR-TDI	Nonlinear	Multiplicative log-normal

Table 3: Characteristics of the test problems.

3.6.1. Logistic Growth The logistic growth equation is a well-known differential equation that has an exact solution. Classically, it was developed to describe population growth at rate r with a carrying capacity K , $\dot{u} = ru(1 - \frac{u}{K})$ [65]. We have reparameterized this equation to the form seen in Equation (21) to be amenable to optimization.

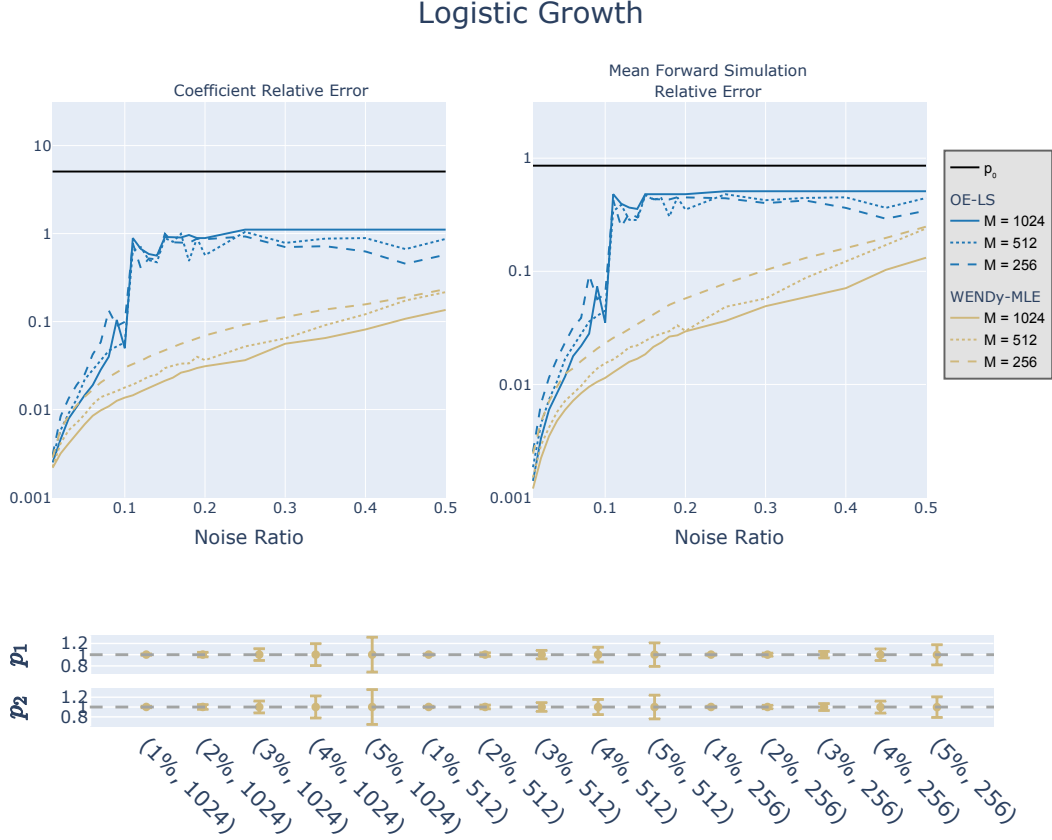


Figure 2: Both algorithms are run at noise ratios from 1% to 50% and $M = \{256, 512, 1024\}$ for a fixed time $T = 10$. The top row plots accuracy metrics for OE-LS in blue, WENDy-MLE in gold, and initial parameterization in black. In the bottom plots is the mean parameter estimate and mean 95% confidence intervals for each parameter estimated by WENDy-MLE in gold and the true parameter in gray.

We see that WENDy-MLE is able to recover the parameters to an accuracy of about 20% relative coefficient error even when noise levels are at 50%. On the other hand the forward solver’s performance degrades to errors above 100% for both the coefficient error and forward solve error. Investigation of this phenomena demonstrated that the degradation in the OE-LS algorithm was primarily caused by corruption of the initial condition. Because the noise is additive, the data for the initial condition \mathbf{u}_0 can become negative. When this occurs, OE-LS cannot reliably navigate in the cost space back to $\hat{\mathbf{u}}_0 > 0$. In contrast, WENDy-MLE does not suffer from this complication, and even when the initial condition is corrupted to a non-physical negative value.

The median across all parameters for estimated relative squared bias, variance, and mean squared error are 0.0033%, 0.129%, 0.259% respectively. The median coverage across all parameters is 100%. These metrics are plotted in the appendix in Figure D1 and are shown in Tables D1 and D2 in the Appendix. The bias, variance and MSE are particularly low for the WENDy-MLE solver. The main driver in MSE is the bias that is caused by the nonlinearity in the RHS \mathbf{f} of the state variable \mathbf{u} . The coverage

demonstrates that WENDy-MLE overestimates the uncertainty of its estimate which is preferable to the alternative. For this example the WENDy-MLE algorithm significantly outperforms the the forward based solver, and as the noise increases, all metrics degrade gracefully.

3.6.2. Hindmarsh Rose The Hindmarsh-Rose Model was initially developed to explain neuronal bursting [22]. Both state variables u_1 and u_2 demonstrate this bursting. Estimation of the parameters is complicated by the differences in scales. In particular, $p_6^* = -50$ and $p_9^* = 0.0318$ which are separated by three orders of magnitude. The WENDy-MLE algorithm use of the likelihood addresses this concern.

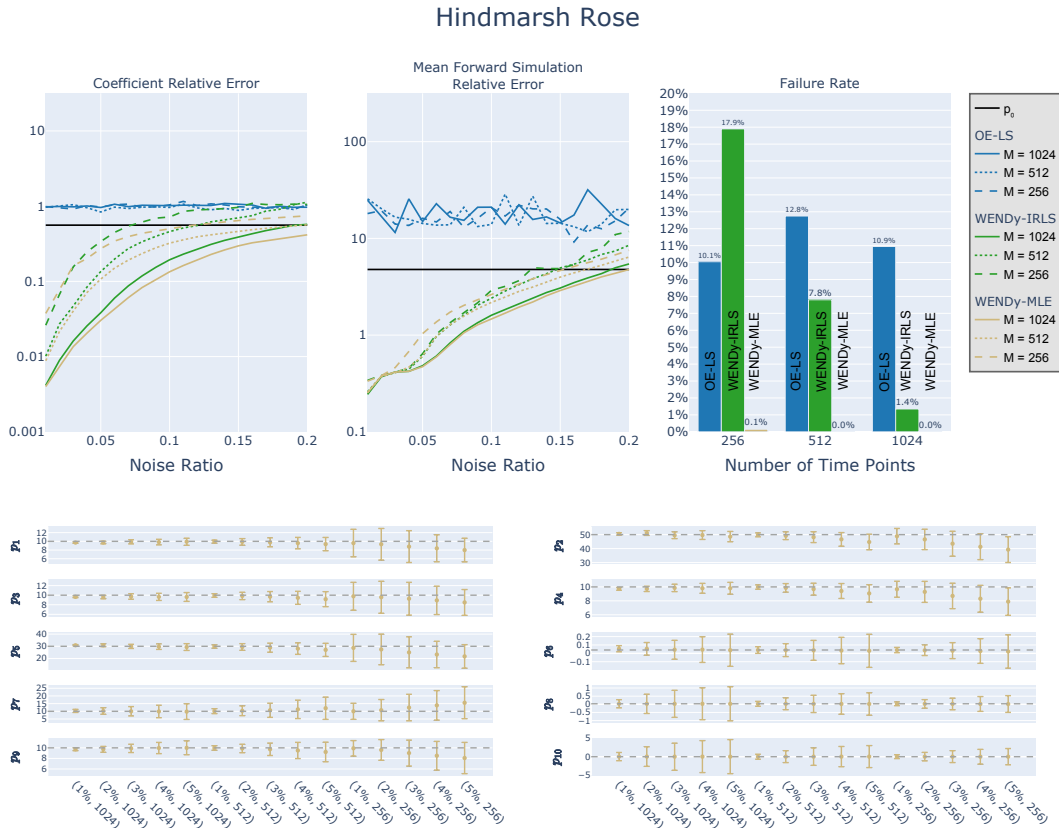


Figure 3: All algorithms are run at noise ratios from 1% to 20% and $M = \{256, 512, 1024\}$. In plots of the top row, we see accuracy metrics for for OE-LS in blue, WENDy-IRLS in green, WENDy-MLE in gold, and initial parameterization in black. In the bottom plots, we see the WENDy-MLE’s mean parameter estimate and mean 95% confidence intervals for each parameter in gold and the true parameter is in gray.

An initial motivation for this work was to improve performance on this example because WENDy-IRLS does not always converge, especially with less data and high noise, $\sigma_{nr} \gg 0$. The likelihood approach described here shows a mild improvement in accuracy metrics over the generalized least squares approach, but its real benefit is the improvement on convergence.

The median across all parameters for estimated relative squared bias, variance, and mean squared error are 13.7%, 0.708%, 17.5% respectively. The median coverage across all parameters is 96.5%. In the appendix, these metrics are shown in Figure D2 and in Tables D3, D4, D5, and D6. For this example the WENDy-MLE algorithm has a bias that affects the MSE for all parameters. Bias stays below 25% for a noise ratio less than 10% for all subsampling rates for all parameters except p_8, p_9 and p_{10} . Those parameters suffer from a lack of identifiability mentioned in [5] which comes from adding noise proportional to $\|\bar{\mathbf{u}}\|$ rather than having noise be anisotropic across state components.

Coverage at noise ratios below 5% stays above 90% for all variables. Uncertainty estimates for p_8, p_9 and p_{10} stay sufficiently high resulting in a coverage $>95\%$ for all noise levels in these parameters. On the other hand, the other parameters all have coverage rates monotonically decrease as the noise ratio increase. This is because Proposition 2 is inapplicable when the noise is not sufficiently small. The linearization used to obtain the weak likelihood becomes a worse estimate for the true likelihood as the noise ratio increases. Also, when the data rate becomes sparser (smaller M) the coverage also degrades. Since the solution to the Hindmarsh system has discontinuities, having sufficient data around these events is paramount for any estimation method.

3.6.3. Lorenz The Lorenz system is a canonical chaotic system that was discussed in more depth in Section 3.5. Here we are running the WENDy-MLE and OE-LS algorithms on this system of ODEs and looking more broadly at how WENDy-MLE compares to the forward based solver in a variety of conditions.

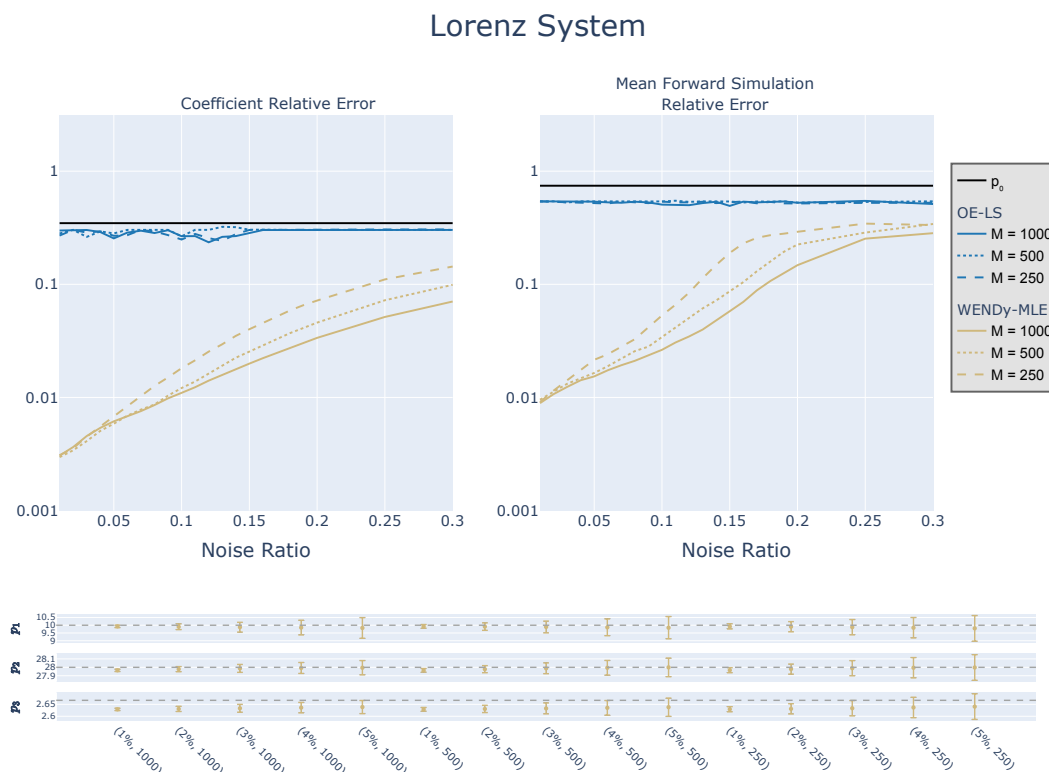


Figure 4: Both algorithms are run at noise ratios from 1% to 30% and $M = \{256, 512, 1024\}$. In plots of the top row, we see accuracy metrics for for OE-LS in blue, WENDy-IRLS in green, WENDy-MLE in gold, and initial parameterization in black. In the bottom plots, we see the WENDy-MLE’s mean parameter estimate and mean 95% confidence intervals for each parameter in gold and the true parameter is in gray.

The median of performance of the forward solver is considerably worse than WENDy-MLE’s, consistent across all noise and sampling levels. The median across all parameters for estimated relative squared bias, variance, and mean squared error are 0.00317%, 0.00565%, 0.0182% respectively. The median coverage across all parameters is 100%. More detailed results are shown in Figure D3 and in Tables D7 and D8 in the Appendix. The bias, variance, and MSE all are reasonable for this problem, all staying below 20% for all parameters at all noise levels. Interestingly, coverage is poor at low noise levels, and improves for moderate noise levels, only to then degrade again for noise levels greater than 16%. We hypothesize this is because numerical error in the forward simulation is on a similar level as the additive noise, hence the Gaussian assumption about the noise is less valid at these noise levels. Once the error is dominated by the additive Gaussian noise, then the covariance produced by WENDy-MLE improves.

3.6.4. Goodwin 2D A simple example of a system of differential equations which is nonlinear in parameters is the Goodwin model which describes negative feedback

control processes [9, 15]. This example was chosen because of the nonlinear right hand side. In particular, the right hand side contains a rational function known in the mathematical biology literature as a Hill function [21, 16]. The parameter p_2 appears in the denominator, and thus this serves as an example of how nonlinearity can effect the performance of the WENDy-MLE algorithm.

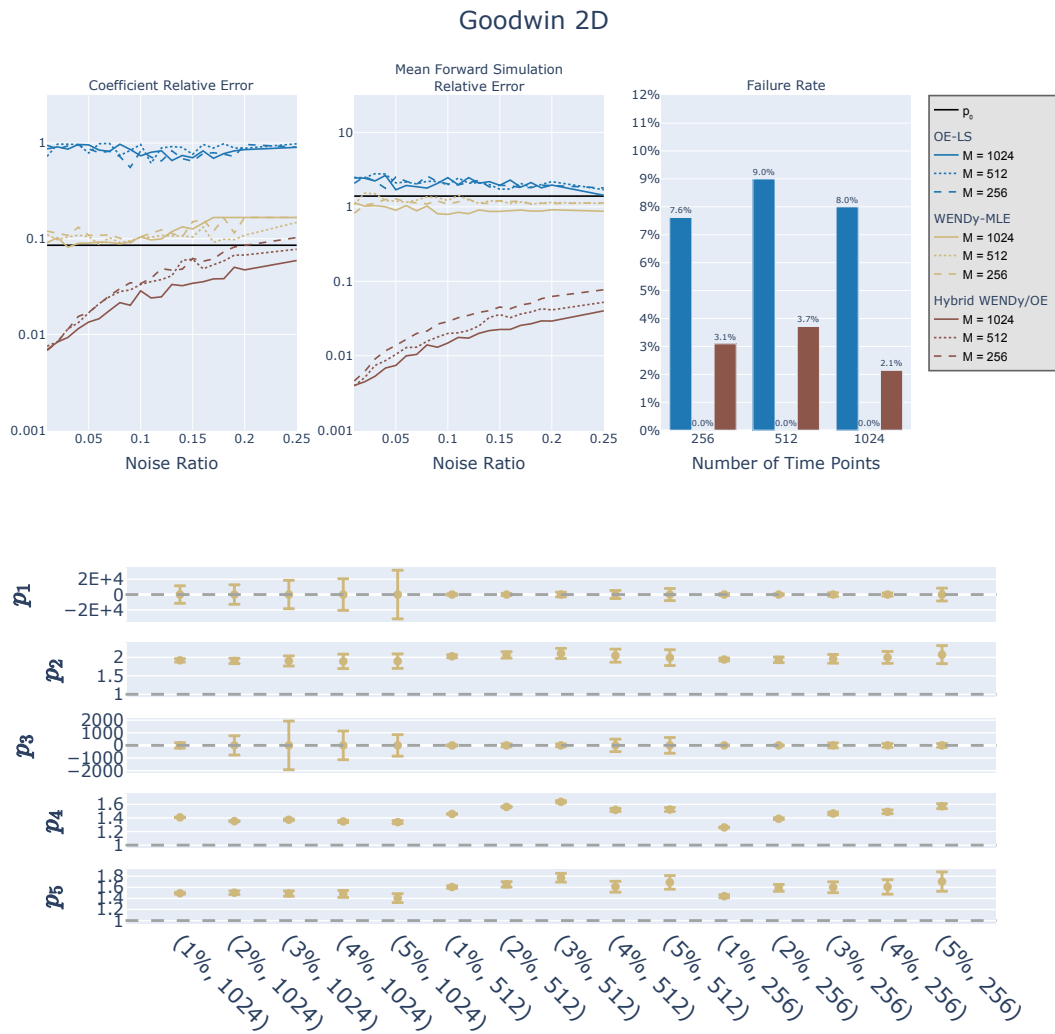


Figure 5: All algorithms are run at noise ratios from 1% to 25% and $M = \{256, 512, 1024\}$. In plots of the top row, we see accuracy metrics for for OE-LS in blue, WENDy-MLE in gold, the hybrid approach in maroon, and initial parameterization in black. In the bottom plots, we see the WENDy-MLE’s mean parameter estimate and mean 95% confidence intervals for each parameter in gold and the true parameter is in gray.

In the this example, we see that the OE-LS algorithm on median has coefficient and forward solve error much worse than the error from the initial guessed parameterization. Furthermore, the OE-LS method has failure rates above five percent for all subsample

rates. Also, WENDy-MLE on median chooses parameters that degrade the coefficient error, but it improves the forward solve error compared to the initial parameterization.

Interestingly enough, the two algorithms have complementary strengths, and it is possible to pair them together to get better results. Specifically, we create a “hybrid” approach that first uses WENDy-MLE to estimate parameters, which are then used as an initial guess for the OE-LS algorithm. As evident in the figure, this hybrid approach greatly improves on either standalone method with respect to both error metrics.

The median across all parameters for estimated relative squared bias, variance, and mean squared error are 13.5%, 29.1%, 86.1% respectively. The median coverage across all parameters is 50%. These metrics are shown in the Appendix in Figure D4 and in Tables D9 and D10. Variance for this problem drives the increase in MSE. Upon inspection of the cost space, we found that there are multiple local minimum in the parameter range explored. This causes WENDy-MLE to converge to different local optimum depending on initialization. The output error method also suffers from a multimodal cost space, and WENDy-MLE’s cost space has a large basin around the minimum closes to truth.

The complications from multimodality spill over and effect coverage. Specifically, for p_2, p_4 , and p_5 the coverage is poor. Another possible source of error could be from the nonlinearity of \mathbf{f} in p_2 . This coupled through a connection u_2 causes degradation in metrics for p_4 and p_5 as well. It is known that estimating p_1, p_2 jointly can cause identifiability problem, as the ratio of numerator and denominator can be balanced rather than converging to the true values. Coverage for all parameters improves as the noise level increased, so it could be that there is insufficient information on this time interval to recover this parameter. It is interesting that this causes problems with estimating p_4 and p_5 .

3.6.5. Goodwin 3D A slightly more complicated version of the Goodwin model is shown in Equation (25). We see that algorithms are now estimating the hill coefficient, p_4 , in the exponent of the state variable. For $p_4^* = 10$ sinusoidal oscillations occur in the state variables, while smaller values do not exhibit this behavior [14].

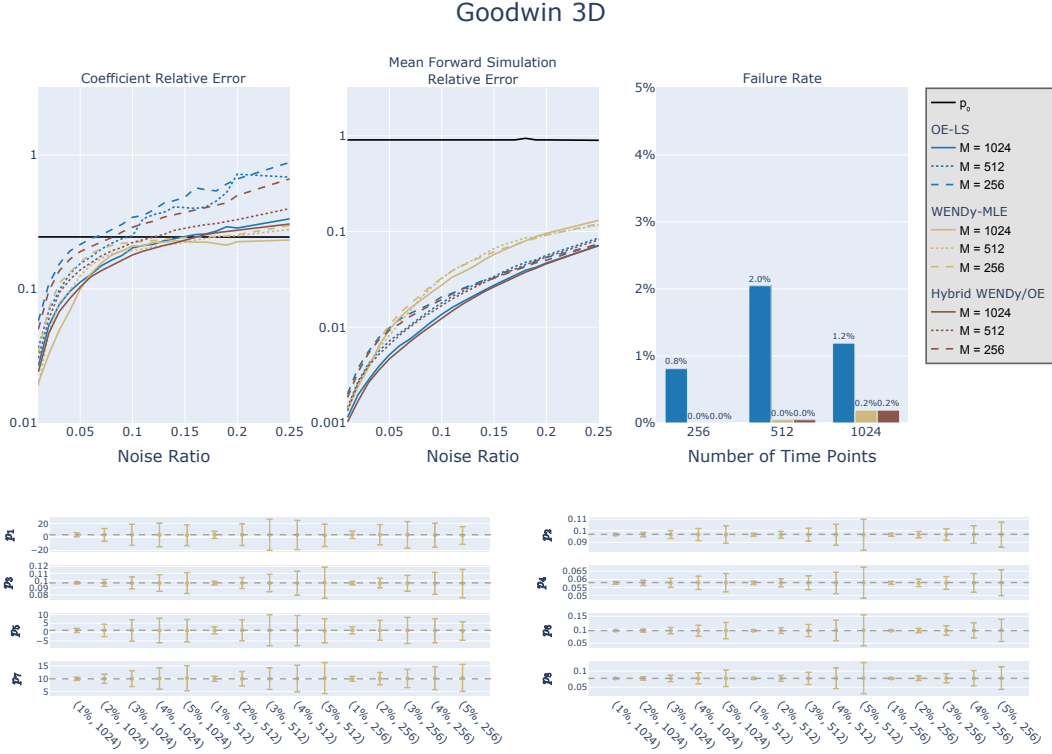


Figure 6: Both algorithms are run at noise ratios from 1% to 25% and $M = \{256, 512, 1024\}$. In plots of the top row, we see accuracy metrics for for OE-LS in blue, WENDy-IRLS in green, WENDy-MLE in gold, and initial parameterization in black. In the bottom plots, we see the WENDy-MLE’s mean parameter estimate and mean 95% confidence intervals for each parameter in gold and the true parameter is in gray

Both algorithms perform reasonably well on this example, but we see that WENDy-MLE outperforms the OE-LS on coefficient error while OE-LS outperforms WENDy-MLE slightly on forward simulation error. When the hybrid approach is used, it has comparable results to the OE-LS method alone. While the forward solve method does not fail as often as on the two dimensional Goodwin example, there still are cases where we saw the forward solver fail. It was surprising that the WENDy-MLE algorithm performed this well because moving to the log-normal noise distribution further adds more nonlinearity to the cost function, so it was expected that the WENDy-MLE algorithm would be more limited in its effectiveness. It is also surprising that using WENDy-MLE as an initialization significantly improves on the performance of the forward based solver. Upon inspection, this is because the WENDy-MLE optimum is often within a domain of convergence for the forward based solver.

The median across all parameters for estimated relative squared bias, variance, and mean squared error are 0.0357%, 0.403%, 0.891% respectively. The median coverage across all parameters is 100%. The metrics for each parameter are shown in Figure D5 and Tables D11, D12, D13 D14, and D15 in the Appendix. Bias drives the MSE for this

example caused by the nonlinearity of \mathbf{f} in both \mathbf{u} and \mathbf{p} . In particular, p_3 exhibits the largest bias nearly reaching 100%. This parameter mirrors p_2 in the previous example, and struggles from the same identifiability problem. It was surprising the metrics improved for the three dimensional Goodwin example. Because log-normal noise is used here, the magnitude of the noise is now proportional to each state u_d . Thus, the noise is anisotropic after the transformation, and this leads to the parameters connected to u_3 more identifiable.

Coverage is particularly good for this example. Only the coverage for p_1 and p_3 ever falls below 95%. This is somewhat surprising because this is an more complicated version of the system described in Equation (24). The dynamics for the parameters in the previous example are on smaller time scales than here, thus making estimating the parameters for the Equation (25) more obtainable.

3.6.6. SIR-TDI The susceptible-infected-recovered (SIR) model is pervasive in epidemiology. The system described in Equation (26) described an extension that allows for time delayed immunity (TDI) for parasitic diseases where there is a common source for infection [60].

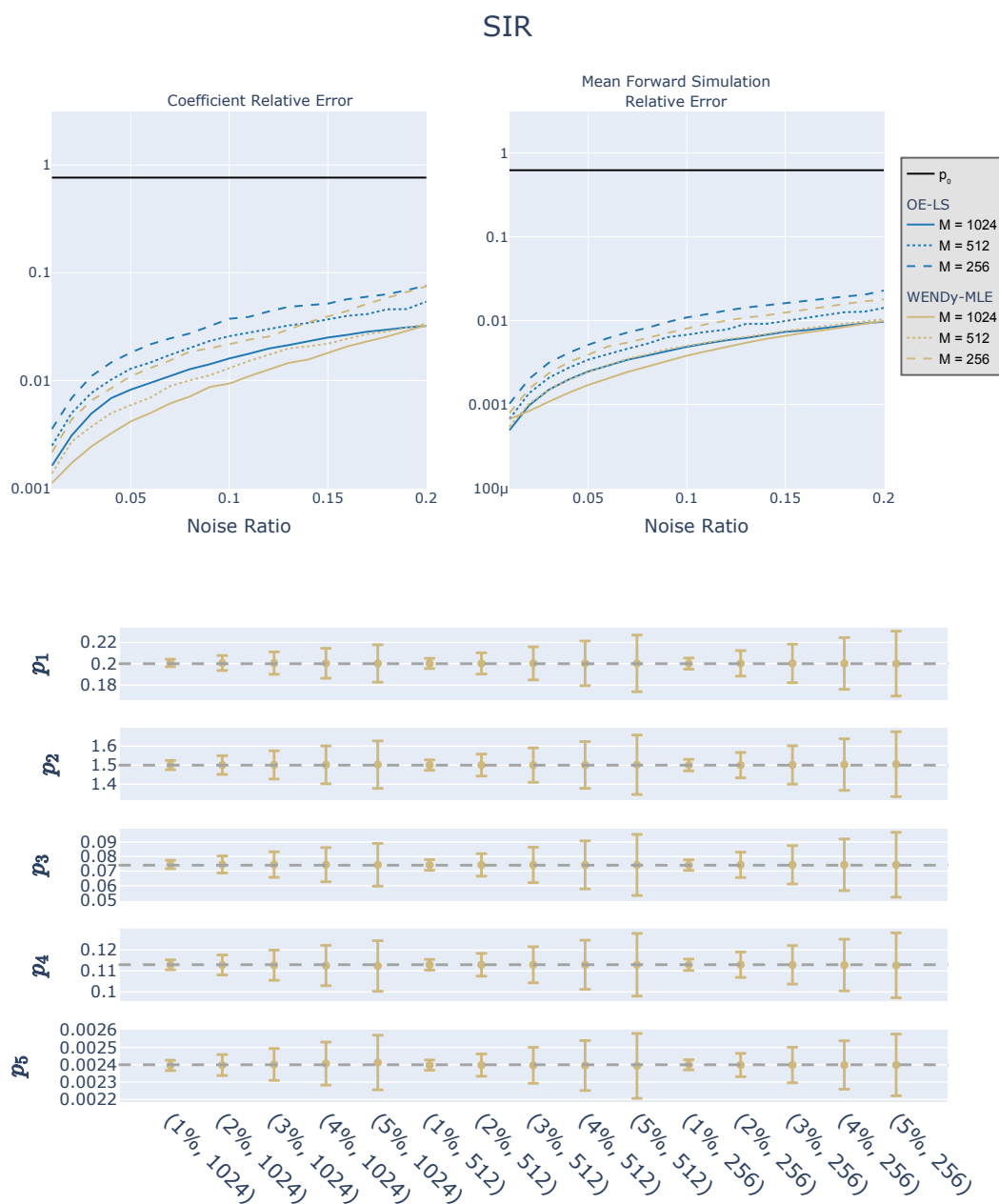


Figure 7: Both algorithms are run at noise ratios from 1% to 20% and $M = \{256, 512, 1024\}$. In plots of the top row, we see accuracy metrics for for OE-LS in blue, WENDy-MLE in gold, and initial parametrization in black. In the bottom plots, we see the WENDy-MLE’s mean parameter estimate and mean 95% confidence intervals for each parameter in gold and the true parameter is in gray

Both algorithms perform well on this example on both metrics. WENDy-MLE slightly outperforms the forward solver based method, but as the noise level increases the gap between the two algorithms’ performance decreases. It is noteworthy to mention at first the WENDy-MLE algorithm was run without constraints, but for this example in particular WENDy-MLE’s performance was much worse. This is most likely due

to the non-linearity in the cost space caused by the highly nonlinear right hand side of Equation (26). The nonlinearity is further exacerbated by multiplicative log-normal noise which requires applying logarithms on both sides of the equation as described in Section 2.6.

The median across all parameters for estimated relative squared bias, variance, and mean squared error are 0.00438%, 0.0581%, 0.146% respectively. The median coverage across all parameters is 100%. These metrics are shown in Figure D6 and in Tables D16 and D17 in the Appendix. Bias, variance and MSE are all below 5% for all parameters and subsamplings (values of M) except for p_5 and $M = 256$ at noise ratios larger than 15%. p_5 is a nonlinear parameter that is an exponential rate. Its true value of 0.0024 is relatively small compared to the other parameters in this system. With less data and higher noise, it is not surprising that this parameter becomes harder to identify.

We over estimate the uncertainty in the covariance on every estimate of for this example resulting in a coverage larger than the nominal 95% for all parameters across the board. While this implies that our confidence intervals are likely larger than necessary, we note again that higher-than-nominal coverage is preferable to the alternative.

4. Discussion

The WENDy-MLE algorithm presented here addresses a more general class of problems than the previous WENDy-IRLS in [5]. In particular, WENDy-MLE can handle systems of ODEs which are nonlinear in the parameters. Furthermore, our method can leverage the distribution for both cases of additive Gaussian Noise and multiplicative log-normal noise. Overall, the WENDy-MLE algorithm estimates parameters more accurately and fails less often than previous weak form methods.

In Table 4, we summarize a qualitative takeaways from our numerical experimentation.

Algorithm	Chaotic	Nonlinear In Parameters	Noise		
			Noiseless	Gaussian	LogNormal
OE-LS	✗ [†]	✓	✓	✓	✓
W-LS	✓	✗ [‡]	✓✓	✗	✗ [‡]
WENDy-IRLS	✓✓	✗ [‡]	✓ [§]	✓	✗ [‡]
WENDy-MLE	✓✓	✓✓	✓ [§]	✓✓	✓✓

Table 4: Here we provide high-level advice on the performance of the discussed methods applied to different classes of problems. We compare OE-LS, solving ordinary least squares for the weak residual (W-LS), WENDy-IRLS, and WENDy-MLE. A double check ✓✓ indicates the algorithm excels under most circumstances in our testing. A single ✓ suggests that the algorithm can work, but requires oversight due to a reduced domain of convergence for initial parameter estimates as well as other numerical discretization challenges. An ✗ indicates that the algorithm is not suited to the problem (e.g., W-LS and WENDy-IRLS only work for linear-in-parameter ODEs and without correction, noisy data will incur bias for W-LS).

There are known limitations to our approach. First, WENDy-MLE is based on maximizing the likelihood of the weak form residual. Accordingly, the form of the ODE must be such that integration-by-parts is possible. We also assume that the measurement noise is either additive Gaussian noise or multiplicative log-normal noise. We also require that all state variables are observed, which is not widely true in many applications. Another limitation is that we assume observational data is provided on a uniform grid, though in principle, there is nothing inhibiting extension to the non-uniform case with a different quadrature rule. Finally, like almost all other methods that do general parameter estimation, we face a non-convex optimization problem for which we cannot guarantee finding the global minimizer for arbitrary initialization. Thus, in

[†] OE-LS can work on short time horizons but in general should not be used for chaotic systems.

[‡] In the Julia implementation, both of these algorithms have been extended by replacing the least square problems with a nonlinear least squares problems. Similarly, the infrastructure makes it possible to run these algorithms with log-normal noise as well.

[§] Because WENDy-IRLS and WENDy-MLE assume measurement noise is present, computation of the covariance is ill-posed for noiseless data. Our software implementation automatically switches to W-LS in this case. In some instance we have seen that incorporating covariance information to estimate parameters for noiseless data can be superior to W-LS. We conjecture the algorithms may be correcting for the numerical error in the solver that generated the artificial data, but this remains a topic for future research.

^{||} For the vast majority of the examples, the domain of convergence is substantially larger than for OE-LS. However, as with all iterative methods, WENDy-MLE benefits from wise initial parameter estimates.

practice it is often necessary to initialize multiple times for best results.

4.1. Robustness in the Presence of Noise

Like other weak form methods, the true strength of the approach lies in the ability to perform well in the presence of noise¶. No pre-processing or smoothing of input data is necessary for the algorithm to be successful in the presence of noise. Instead, the set of test functions that are chosen when forming Φ and $\dot{\Phi}$ are built adaptively from the data as described in [Appendix A.1.1](#). Furthermore, relying on the intuition from theoretical results, the discrete weak form residual is analogous to considering the continuous weak form solution. This means that our method is relying on a more relaxed topology, and this leads to algorithms with a cost space that is smoother and more easily navigable.

4.2. Bias

One known limitation of our method is that the asymptotic expansion in [Proposition 2](#) is only valid in a neighborhood about $\mathbf{0}$. In practice, this neighborhood shrinks as the nonlinearity of the right hand side, \mathbf{f} , becomes more severe. These non-zero higher order terms lead WENDy to a bias that increases in magnitude with the noise. In the best case, if we obtain a minimum in the linear part of \mathbf{r}^ϵ , the expectation of these higher order terms will be non-zero, leading to a bias in our estimator.

In [Figure 8](#), the Goodwin 3D (shown in [Equation \(25\)](#)) is run with all other parameters fixed to their true values except for p_4 and p_5 at 100 simulated datasets for each different level of noise. The likelihoods are averaged over the runs to produce the contours shown. As the noise ratio is increased, the local optimum is shifted away from truth. This is caused by the nonlinear terms that are neglected in [Proposition 2](#). As the noise becomes larger, the nonlinear terms cause a bias in the WENDy estimate.

4.3. Computational Cost

A strength of the weak form methods is that no forward simulation is necessary at each step of the optimization routine. When the system of differential equations is small and not stiff, then standard forward solve methods may be more efficient and the main benefit to using a weak form method like ours is that of robustness to both noise and to poor initialization. However, as the dimensionality of state variables and stiffness of the problem increases, the forward solves become more computationally expensive, whereas WENDy-MLE is unaffected.

Recall that K is the number of test functions, $M + 1$ is the number of time points, D is the dimension of the state variable \mathbf{u} , and J is the dimension of the parameters \mathbf{p} . Computing the weak form negative log-likelihood itself has a complexity of $\mathcal{O}(K^2 D^3 (MJ + K))$. Similarly, the gradient computation has a complexity of $\mathcal{O}(K^2 D^2 (D(MJ + K) + J))$ and the Hessian computation has a complexity of

¶ Smoothing can help (up to a point), see [\[38\]](#).

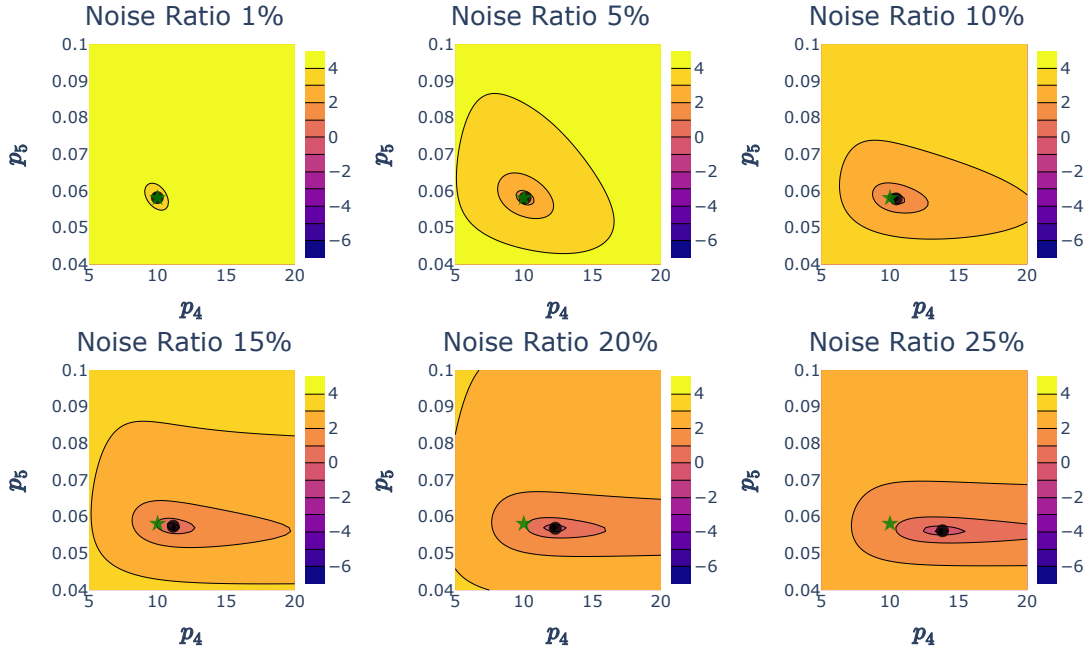


Figure 8: The WENDy algorithm is run on the Goodwin 3D problem with all parameters fixed to truth except p_4 and p_5 for a variety of noise levels. The truth is shown as a green star, and the WENDy optimum is identified with a black circle. One can notice that the optimum moves further from truth as noise increases.

$\mathcal{O}(K^2 D^2 (D(MJ + K) + J^2))$. The most expensive step in our method is computing the derivatives of the weak form log-likelihood for the second order optimization methods. Our implementation meticulously caches as much as possible, pre-allocates memory, applies an advantageous order of operations, and uses efficient data structures.

In the linear case, many of the operators either become constant matrices or tensors that can be thought of as linear operators. Also, some operators are zero due to higher order derivatives being applied to the linear function. This reduces the constants involved in the cost, but incurs the same asymptotic complexity as the nonlinear case. One can see that the dominant cause for the cost is due to the number of test functions in Figure 9. Notice that the recorded run times shown in Figure 9a approximately match the predicted cost of the line of slope 1.

The example above has ten parameters ($J = 10$). Because the cost is dominated by the mat-mat computations for matrices of size KD , the gradient computation takes approximately an order of magnitude more time, and the Hessian takes an order of magnitude more than the gradient.

Figure 9 shows the computational cost for different sized problems. Problems that are linear in parameters show a decrease in the computational cost but only by a scaling factor. The experiment verifies the cost of the algorithm scales linearly with respect to the number of data points on the grid and cubically with respect to the number of test functions. Unlike OE methods, the weak form methods can control the computational

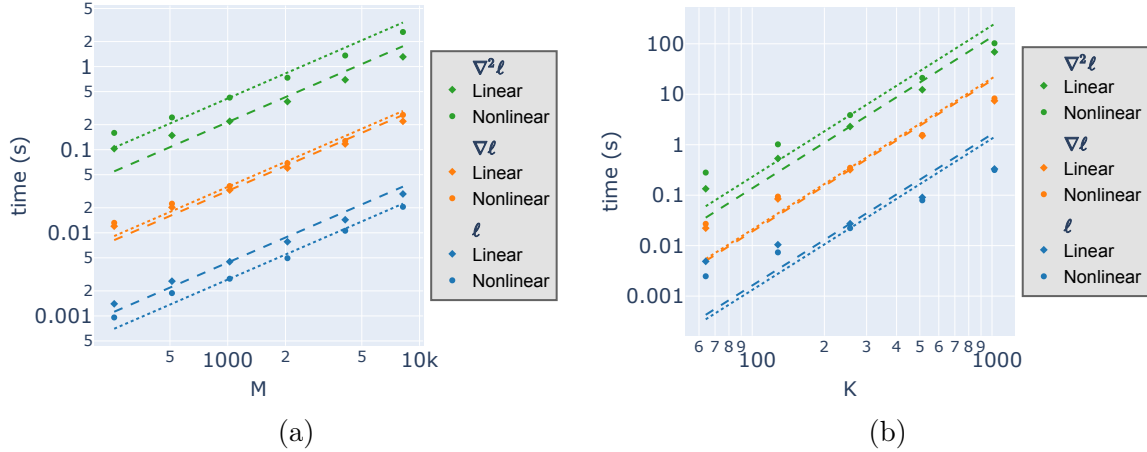


Figure 9: On the left, K, D, J are all fixed, and M is varied. On the right, M, D, J are all fixed, and K is varied. The dashed and dotted lines correspond to a linear fit with a fixed slope ($\mathcal{O}(M), \mathcal{O}(K^3)$ respectively). Both plots are show on a log-log scale.

cost by using fewer test functions. In practice, we used 200-500 test functions which results in reasonable computational cost for the likelihood and its derivatives.

5. Conclusion

In this work, the WENDy algorithm was extended to a more general case of differential equations where the right hand side may be nonlinear in parameters. Furthermore, the approach explicitly supports both additive Gaussian and multiplicative log-normal noise. The likelihood based approach improved on the convergence and accuracy compared to the previous work. Also, the new Julia implementation improved the usability and efficiency of the algorithm.

The likelihood derived is limited by the linearization used. Further investigation of higher order expansions or other derivation strategies are necessary to handle high nonlinearities and noise levels. The computational advantage of the approach should be more apparent in the extension of the algorithm to larger systems of ordinary differential equations and partial differential equations. Also, further optimization of test function selection to recover maximum information in the weak form is another area of further exploration.

6. Acknowledgments

The authors would like to thank April Tran (University of Colorado) for insights regarding software development for weak form methods.

This work is supported in part by the National Institute of General Medical Sciences grant R35GM149335, National Science Foundation grant 2109774, National Institute of Food and Agriculture grant 2019-67014-29919, and by the Department of Energy,

Office of Science, Advanced Scientific Computing Research under Award Number DE-SC0023346.

References

- [1] M. Abbott, D. Aluthge, N3N5, V. Puri, C. Elrod, S. Schaub, C. Lucibello, J. Bhattacharya, J. Chen, K. Carlsson, and M. Gelbrecht. Mcabbott/Tullio.jl: V0.3.7. Zenodo, Oct. 2023.
- [2] A. Aldoghaither, D.-Y. Liu, and T.-M. Laleg-Kirati. Modulating Functions Based Algorithm for the Estimation of the Coefficients and Differentiation Order for a Space-Fractional Advection-Dispersion Equation. *SIAM J. Sci. Comput.*, 37(6):A2813–A2839, Jan. 2015.
- [3] K. Atkinson. *An Introduction to Numerical Analysis*. Wiley, New York, NY, 2nd edition, 1989.
- [4] J. Bezanson, A. Edelman, S. Karpinski, and V. B. Shah. Julia: A Fresh Approach to Numerical Computing. *SIAM Rev.*, 59(1):65–98, Jan. 2017.
- [5] D. M. Bortz, D. A. Messenger, and V. Dukic. Direct Estimation of Parameters in ODE Models Using WENDy: Weak-form Estimation of Nonlinear Dynamics. *Bull. Math. Biol.*, 85(110), 2023.
- [6] D. M. Bortz, D. A. Messenger, and A. Tran. Weak form-based data-driven modeling: Computationally Efficient and Noise Robust Equation Learning and Parameter Inference. In S. Mishra and A. Townsend, editors, *Numerical Analysis Meets Machine Learning*, volume 25 of *Handbook of Numerical Analysis*, pages 54–82. Elsevier, 2024.
- [7] N. J.-B. Brunel, Q. Clairon, and F. d’Alché-Buc. Parametric Estimation of Ordinary Differential Equations With Orthogonality Conditions. *J. Am. Stat. Assoc.*, 109(505):173–185, Jan. 2014.
- [8] S. L. Brunton, J. L. Proctor, and J. N. Kutz. Discovering governing equations from data by sparse identification of nonlinear dynamical systems. *Proc. Natl. Acad. Sci.*, 113(15):3932–3937, Apr. 2016.
- [9] B. Calderhead. *Differential Geometric MCMC Methods and Applications*. PhD thesis, University of Glasgow, 2012.
- [10] P. R. Conrad, Y. M. Marzouk, N. S. Pillai, and A. Smith. Accelerating Asymptotically Exact MCMC for Computationally Intensive Models via Local Approximations. *J. Am. Stat. Assoc.*, 111(516):1591–1607, Oct. 2016.
- [11] V. Dukic, H. F. Lopes, and N. G. Polson. Tracking Epidemics With Google Flu Trends Data and a State-Space SEIR Model. *J. Am. Stat. Assoc.*, 107(500):1410–1426, Dec. 2012.
- [12] J. Durbin. Errors in Variables. *Rev. Int. Stat. Inst.*, 22(1/3):23, 1954.

- [13] J.-P. Dussault, T. Migot, and D. Orban. Scalable adaptive cubic regularization methods. *Math. Program.*, 207(1-2):191–225, Sept. 2024.
- [14] D. Gonze and W. Abou-Jaoudé. The Goodwin Model: Behind the Hill Function. *PLoS ONE*, 8(8):e69573, Aug. 2013.
- [15] B. C. Goodwin. Oscillatory behavior in enzymatic control processes. *Advances in Enzyme Regulation*, 3:425–437, Jan. 1965.
- [16] S. Goutelle, M. Maurin, F. Rougier, X. Barbaut, L. Bourguignon, M. Ducher, and P. Maire. The Hill equation: A review of its capabilities in pharmacological modelling. *Fundamental Clinical Pharma*, 22(6):633–648, Dec. 2008.
- [17] S. Gowda, Y. Ma, A. Cheli, M. Gwózzdź, V. B. Shah, A. Edelman, and C. Rackauckas. High-performance symbolic-numeric via multiple dispatch. *ACM Commun. Comput. Algebra*, 55(3):92–96, Sept. 2021.
- [18] H. Greenberg. A survey of methods for determining stability parameters of an airplane from dynamic flight measurements. Technical Report NACA TN 2340, Ames Aeronautical Laboratory, Moffett Field, CA, Apr. 1951.
- [19] D. R. Gurevich, P. A. K. Reinbold, and R. O. Grigoriev. Robust and optimal sparse regression for nonlinear PDE models. *Chaos*, 29(10):103113, Oct. 2019.
- [20] P. Hall and Y. Ma. Quick and easy one-step parameter estimation in differential equations. *J. R. Stat. Soc. B*, 76(4):735–748, Sept. 2014.
- [21] A. V. Hill. The possible effects of the aggregation of the molecules of haemoglobin on its dissociation curves. *J. Physiol.*, 40(suppl):iv–vii, Dec. 1910.
- [22] J. L. Hindmarsh and R. M. Rose. A model of neuronal bursting using three coupled first order differential equations. *Proc R Soc Lond B Biol Sci*, 221(1222):87–102, Mar. 1984.
- [23] T. Janiczek. Generalization of the modulating functions method into the fractional differential equations. *Bull. Pol. Acad. Sci. Tech. Sci.*, 58(4), Jan. 2010.
- [24] J. Jouffroy and J. Reger. Finite-time simultaneous parameter and state estimation using modulating functions. In *2015 IEEE Conf. Control Appl. CCA*, pages 394–399, Sydney, Australia, Sept. 2015. IEEE.
- [25] P. K. Mogensen and A. N. Riseth. Optim: A mathematical optimization package for Julia. *JOSS*, 3(24):615, Apr. 2018.
- [26] D. A. Kennedy, V. Dukic, and G. Dwyer. Pathogen Growth in Insect Hosts: Inferring the Importance of Different Mechanisms Using Stochastic Models and Response-Time Data. *Am. Nat.*, 184(3):407–423, Sept. 2014.
- [27] T. G. Kolda and B. W. Bader. Tensor Decompositions and Applications. *SIAM Review*, 51(3):455–500, Aug. 2009.
- [28] C.-S. Liu, J.-R. Chang, and Y.-W. Chen. The recovery of external force in nonlinear system by using a weak-form integral method. *Nonlinear Dyn.*, 86(2):987–998, Oct. 2016.

- [29] D.-Y. Liu and T.-M. Laleg-Kirati. Robust fractional order differentiators using generalized modulating functions method. *Signal Processing*, 107:395–406, Feb. 2015.
- [30] L. Ljung. *System Identification: Theory for the User*. Prentice Hall Information and System Sciences Series. Prentice Hall PTR, Upper Saddle River, NJ, 2nd edition, 1999.
- [31] L. Ljung. *System Identification*, pages 1–19. John Wiley & Sons, Inc., Hoboken, NJ, USA, May 2017.
- [32] J. M. Loeb and G. M. Cahen. Extraction a partir des enregistrements de mesures, des parametres dynamiques d’un systeme. *Automatisme*, 8:479–486, 1965.
- [33] J. M. Loeb and G. M. Cahen. More about process identification. *IEEE Trans. Autom. Control*, 10(3):359–361, July 1965.
- [34] K. McGoff, S. Mukherjee, and N. Pillai. Statistical inference for dynamical systems: A review. *Stat. Surv.*, 9:209–252, Jan. 2015.
- [35] D. A. Messenger and D. M. Bortz. Weak SINDy For Partial Differential Equations. *J. Comput. Phys.*, 443:110525, Oct. 2021.
- [36] D. A. Messenger and D. M. Bortz. Weak SINDy: Galerkin-Based Data-Driven Model Selection. *Multiscale Model. Simul.*, 19(3):1474–1497, 2021.
- [37] D. A. Messenger and D. M. Bortz. Learning mean-field equations from particle data using WSINDy. *Physica D*, 439:133406, Nov. 2022.
- [38] D. A. Messenger and D. M. Bortz. Asymptotic consistency of the WSINDy algorithm in the limit of continuum data. *IMA J. Numer. Anal.*, page drae086, Dec. 2024.
- [39] D. A. Messenger, J. W. Burby, and D. M. Bortz. Coarse-Graining Hamiltonian Systems Using WSINDy. *Sci. Rep.*, 14(14457):1–24, 2024.
- [40] D. A. Messenger, E. Dall’Anese, and D. M. Bortz. Online Weak-form Sparse Identification of Partial Differential Equations. In *Proc. Third Math. Sci. Mach. Learn. Conf.*, volume 190 of *Proceedings of Machine Learning Research*, pages 241–256. PMLR, 2022.
- [41] D. A. Messenger, A. Tran, V. Dukic, and D. M. Bortz. The Weak Form Is Stronger Than You Think. *SIAM News*, 57(8), Oct. 2024.
- [42] D. A. Messenger, G. E. Wheeler, X. Liu, and D. M. Bortz. Learning Anisotropic Interaction Rules from Individual Trajectories in a Heterogeneous Cellular Population. *J. R. Soc. Interface*, 19(195):20220412, Oct. 2022.
- [43] T. Migot, D. Orban, and A. Soares Siqueira. JSOSolvers.jl: JuliaSmoothOptimizers optimization solvers. Zenodo, Oct. 2024.
- [44] J. T. Nardini and D. M. Bortz. The influence of numerical error on parameter estimation and uncertainty quantification for advective PDE models. *Inverse Probl.*, 35(6):065003, May 2019.

- [45] A. Pal, F. Holtorf, A. Larsson, T. Loman, Utkarsh, F. Schaefer, Q. Qu, A. Edelman, and C. Rackauckas. NonlinearSolve.jl: High-Performance and Robust Solvers for Systems of Nonlinear Equations in Julia. *arXiv:2403.16341*, Mar. 2024.
- [46] Y. Pantazis and I. Tsamardinos. A unified approach for sparse dynamical system inference from temporal measurements. *Bioinformatics*, 35(18):3387–3396, Sept. 2019.
- [47] A. Patra and H. Unbehauen. Identification of a class of nonlinear continuous-time systems using Hartley modulating functions. *Int. J. Control*, 62(6):1431–1451, Dec. 1995.
- [48] A. E. Pearson and F. C. Lee. Parameter identification of linear differential systems via Fourier based modulating functions. *Control-Theory Adv. Technol.*, 1(4):239–266, Dec. 1985.
- [49] G. Pin, A. Assalone, M. Lovera, and T. Parisini. Non-Asymptotic Kernel-Based Parametric Estimation of Continuous-time. *IEEE Trans. Automat. Contr.*, pages 1–1, 2015.
- [50] G. Pin, B. Chen, and T. Parisini. Robust finite-time estimation of biased sinusoidal signals: A volterra operators approach. *Automatica*, 77:120–132, Mar. 2017.
- [51] C. Rackauckas and Q. Nie. DifferentialEquations.jl – A Performant and Feature-Rich Ecosystem for Solving Differential Equations in Julia. *JORS*, 5(1):15, May 2017.
- [52] J. O. Ramsay, G. Hooker, D. Campbell, and J. Cao. Parameter estimation for differential equations: A generalized smoothing approach. *J. R. Stat. Soc. Ser. B Stat. Methodol.*, 69(5):741–796, Nov. 2007.
- [53] P. Regalia. An unbiased equation error identifier and reduced-order approximations. *IEEE Trans. Signal Process.*, 42(6):1397–1412, June 1994.
- [54] J. Revels, M. Lubin, and T. Papamarkou. Forward-Mode Automatic Differentiation in Julia. *arXiv:1607.07892*, July 2016.
- [55] S. H. Rudy, S. L. Brunton, J. L. Proctor, and J. N. Kutz. Data-driven discovery of partial differential equations. *Sci. Adv.*, 3(4):e1602614, Apr. 2017.
- [56] B. P. Russo, D. A. Messenger, D. M. Bortz, and J. A. Rosenfeld. Weighted Composition Operators for Learning Nonlinear Dynamics. *IFAC-PapersOnLine*, 58(17):97–102, 2024.
- [57] H. Schaeffer. Learning partial differential equations via data discovery and sparse optimization. *Proc. R. Soc. Math. Phys. Eng. Sci.*, 473(2197):20160446, Jan. 2017.
- [58] M. Shinbrot. On the analysis of linear and nonlinear dynamical systems for transient-response data. Technical Report NACA TN 3288, Ames Aeronautical Laboratory, Moffett Field, CA, Dec. 1954.
- [59] M. Shinbrot. On the Analysis of Linear and Nonlinear Systems. *Trans. Am. Soc. Mech. Eng.*, 79(3):547–551, Apr. 1957.

- [60] R. W. Shonkwiler and J. Herod. *Mathematical Biology: An Introduction with Maple and Matlab*. Undergraduate Texts in Mathematics. Springer New York, New York, NY, 2009.
- [61] C. Sparrow. *The Lorenz Equations: Bifurcations, Chaos, and Strange Attractors*, volume 41 of *Applied Mathematical Sciences*. Springer, New York, NY, 1982.
- [62] K. Takaya. The use of Hermite functions for system identification. *IEEE Trans. Autom. Control*, 13(4):446–447, Aug. 1968.
- [63] T. Toni, D. Welch, N. Strelkowa, A. Ipsen, and M. P. Stumpf. Approximate Bayesian computation scheme for parameter inference and model selection in dynamical systems. *J. R. Soc. Interface.*, 6(31):187–202, Feb. 2009.
- [64] A. Tran, X. He, D. A. Messenger, Y. Choi, and D. M. Bortz. Weak-Form Latent Space Dynamics Identification. *Comput. Methods Appl. Mech. Eng.*, 427:116998, July 2024.
- [65] P. F. Verhulst. Notice sur la loi que la population suit dans son accroissement. In J. Garnier and A. Quetelet, editors, *Correspondance Mathématique et Physique*, volume 10, pages 113–121. M.Hayez, imprimeur, 1838.
- [66] Z. Wang, X. Huan, and K. Garikipati. Variational system identification of the partial differential equations governing the physics of pattern-formation: Inference under varying fidelity and noise. *Comput. Methods Appl. Mech. Eng.*, 356:44–74, Nov. 2019.
- [67] S. W. K. Wong, S. Yang, and S. C. Kou. **Magi** : A Package for Inference of Dynamic Systems from Noisy and Sparse Data via Manifold-Constrained Gaussian Processes. *J. Stat. Soft.*, 109(4), 2024.
- [68] S. Yang, S. W. K. Wong, and S. C. Kou. Inference of dynamic systems from noisy and sparse data via manifold-constrained Gaussian processes. *Proc Natl Acad Sci USA*, 118(15):e2020397118, Apr. 2021.

Appendix A. Discretization and Test Functions

In order to satisfy the weak form, a solution must satisfy Eq. (2) for all possible test functions. However, in this work, we are not concerned with the solution itself, but with estimating the parameters in Eq. (2). As the efficacy of the WENDy algorithm depends strongly on wisely choosing test function hyperparameters (smoothness, radius, etc.), in this Appendix we provide an exposition of the test function creation process in [5].

Appendix A.1. Discretization of the Weak Form

Starting from Eq. (2), we must choose a finite set of test functions to create a vector of weak form EE residuals to be minimized. In approaches such as the Finite Element Method, this set is chosen based upon the expected properties of the solution as well as the class of equations being solved. Conversely, to perform weak form EE-based

parameter estimation, we assume the availability of samples of the (possibly noisy) solution. In pursuit of the estimation goal, however, we note that how to optimally choose the properties, number, and location of the test functions remains an open problem. Nonetheless, in [36], it was reported that smoother test functions result in a more accurate convolution integral (via the Euler–Maclaurin formula), while later research revealed that test functions with wider support frequently performed better, and subsequently an algorithm to choose the support size was developed in [35]. These empirical observations regarding smoothness and support size have partially guided the design of the following algorithm.

From a numerical linear algebra perspective, it would be best if the test functions were orthogonal. Towards this goal, we begin by considering the following C^∞ bump function

$$\varphi_k(t; \eta, m_t) = C \exp \left(- \frac{\eta}{\left[1 - \left(\frac{t-t_k}{m_t \Delta t} \right)^2 \right]_+} \right) \quad (\text{A.1})$$

where t_k is the center of the function, m_t controls the radius of the support, the constant C normalizes the test function such that $\|\varphi_k\|_2 = 1$, η is a shape parameter, and $[\cdot]_+ := \max(\cdot, 0)$, so that $\varphi_k(t; m_t \Delta t)$ is supported only on $[-m_t \Delta t, m_t \Delta t]$. Using the algorithm below in [Appendix A.1.1](#), we identify the minimal value for m_t such that the numerical error in the convolution integral does not dominate the residual (denoted as \underline{m}_t). We define the set of test functions to be all test functions such that they are compactly supported over the measured time domain (t_0, t_M) , and have the following features: 1) the t_k values coincide with the sampled timepoints and 2) allowable radii are larger than the minimal one \underline{m}_t . Motivated by empirical results, the shape parameter is arbitrarily fixed at $\eta = 9$. This gives us a set of K_{full} test functions $\{\varphi_k\}_{k=1}^{K_{\text{full}}}$ and we evaluate them on the grid to obtain the matrices:

$$\Phi_{\text{full}} := \begin{bmatrix} \varphi_1(t_0) & \cdots & \varphi_{K_{\text{full}}}(t_0) \\ \vdots & \ddots & \vdots \\ \varphi_1(t_M) & \cdots & \varphi_{K_{\text{full}}}(t_M) \end{bmatrix}, \quad \dot{\Phi}_{\text{full}} := \begin{bmatrix} \dot{\varphi}_1(t_0) & \cdots & \dot{\varphi}_{K_{\text{full}}}(t_0) \\ \vdots & \ddots & \vdots \\ \dot{\varphi}_1(t_M) & \cdots & \dot{\varphi}_{K_{\text{full}}}(t_M) \end{bmatrix}$$

Appendix A.1.1. Minimum Radius Selection. The algorithm by which these test functions are chosen is more fully described in [5], but a short summary is given here.

Our analysis follows the equation $\dot{u} = \mathbf{f}(u)$ where u is a one dimensional state variable. The result is generalized to a D dimensional system by applying the radius selection in each dimension independently. We see that using integration by parts for a test function φ gives the equality $-\langle \dot{\varphi}, u \rangle = \langle \varphi, \mathbf{f}(u) \rangle$. Integrating, we obtain

$$0 = \int_0^T \mathbf{f}(u(t)) \varphi(t) + \varphi'(t) u(t) dt = \int_0^T \frac{d}{dt} (u(t) \varphi(t)) dt.$$

Thus this integral should be zero, or at least small accounting for the presence of numerical error and noise. In this work, we use the trapezoidal rule on a uniform time grid. Because the φ are test functions with compact support on the interior of the domain, we can define the integration error as in Proposition 1:

$$e_{\text{int}}(M) = \frac{T}{M} \sum_{m=0}^M \frac{d}{dt}(u\varphi)(t_m) \quad (\text{A.2})$$

By expanding $\frac{d}{dt}(u(t)\varphi(t))$ into its Fourier Series, where the coefficients are given by $\mathcal{F}_n[\cdot] := \frac{1}{\sqrt{T}} \int_0^T (\cdot) \exp\left[-\frac{2\pi in}{T}t\right] dt$, we can make the following simplification:

$$\begin{aligned} \frac{d}{dt}(u(t)\varphi(t)) &= \sum_{n \in \mathbb{Z}} \mathcal{F}_n \left[\frac{d}{dt}(u(t)\varphi(t)) \right] \exp\left[\frac{2\pi in}{T}t\right] \\ &= \sum_{n \in \mathbb{Z}} \left(\frac{1}{T} \int_0^T \frac{d}{dt}(u(t)\varphi(t)) \exp\left[-\frac{2\pi in}{T}t\right] dt \right) \exp\left[\frac{2\pi in}{T}t\right] \\ &\stackrel{\text{IBP}}{=} \frac{-2\pi i}{T} \sum_{n \in \mathbb{Z}} n \underbrace{\left(\frac{1}{T} \int_0^T u(t)\varphi(t) \exp\left[-\frac{2\pi in}{T}t\right] dt \right)}_{=\mathcal{F}_n[\varphi u]} \exp\left[\frac{2\pi in}{T}t\right]. \end{aligned}$$

The last simplification in the integration by parts relies on the fact that φ is a test function for the domain $[0, T]$, thus $\text{supp}(\varphi) \subset (0, T)$. Now if we return to the quantity of interest, $e_{\text{int}}(M)$, by integrating both sides over the time interval we obtain:

$$e_{\text{int}} = \frac{2\pi i}{M} \sum_{n \in \mathbb{Z}} n \mathcal{F}_n[\varphi u] \underbrace{\sum_{m=0}^M \exp\left[\frac{2\pi ni}{M}m\right]}_{:=I_n}.$$

Notice that $\forall n \neq 0$, I_n is 0 because $\exp\left[\frac{2\pi ni}{M}t\right] dt$ is periodic on $[0, T]$. Also, \mathcal{F}_0 is 0 because it corresponds to the true integral. Notice that when $n = \ell M$ for some integer ℓ , then we have that $I_n = M$ because the quadrature nodes align with the roots of unity for all the Fourier modes. Because the Fourier modes should decay as M gets larger, we can say

$$e_{\text{int}} \approx \text{imag} \left\{ 2\pi n \mathcal{F}_M[\varphi u] \right\}.$$

Because we do not know u analytically, the true Fourier coefficients are approximated by the Discrete Fourier Transform, $\hat{\mathcal{F}}_{n-\lfloor \frac{M}{2} \rfloor}[\mathbf{u}^*] = \frac{T}{M} \sum_{m=0}^M \mathbf{u}_m^* \exp\left[\frac{2\pi in}{M}m\right]$.

Thus, the largest mode we can approximate is the $\lfloor \frac{M}{2} \rfloor$ mode. Also, note that applying the same quadrature rule to a sub-sampled grid gives us an upper bound on the error:

$$e_{\text{int}}(M) \leq e_{\text{int}}\left(\left\lfloor \frac{M}{2} \right\rfloor\right).$$

This motivates subsampling in time to inspect the error. Letting $\tilde{M} := \lfloor \frac{M}{s} \rfloor$ for some scaling factor $s > 2$, we approximate the integration error when subsampled.

The last complication is that we do not have access to \mathbf{u}^* , so we must approximate by substituting \mathbf{u} :

$$e_{\text{int}}(\tilde{M}) \leq \hat{e}_{\text{int}}(\tilde{M}) = \frac{2pi}{\sqrt{T}} \hat{F}_{\tilde{M}}(\mathbf{u}).$$

This motivates us to search over the space of possible radii, and then select the smallest radius possible when the effects due to noise become dominate. Qualitatively, our reasoning is that we can approximate the integration error by using the data, but as noise levels becomes more extreme the effects to noise become dominate for smaller radii, thus for higher noise we expect to select smaller radii in general. This can be seen in Figure A1.

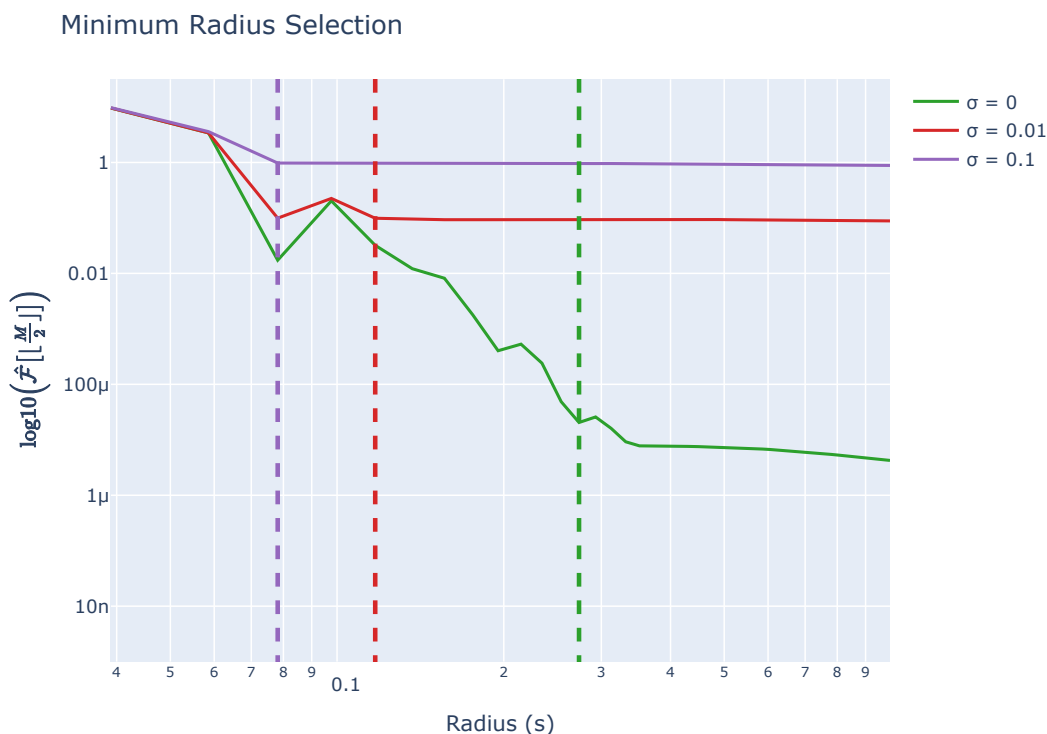


Figure A1: The results for the logistic growth function on the time domain $(0, 10)$, initial condition of 0.01 and $M = 512$, looking at $\hat{\mathcal{F}}_{256}$ for a variety of radii $m_t \in [0.01, 1]$. A vertical line indicates where we have detected a corner in the integration error surrogate

Appendix A.1.2. Reducing the Size of the Test Function Matrix The test function matrix Φ_{full} is often overdetermined, so in order to improve the conditioning of the system we use an SVD reduction technique to obtain a matrix Φ that has a better condition number $\kappa(\Phi) := \sigma_1(\Phi)/\sigma_K(\Phi)$, while still retaining as much information as possible. This is done by looking for a corner in the singular values. Let the SVD of Φ_{full} by

$$\Phi_{\text{full}} = \mathbf{Q} \text{diag}([\sigma_1, \dots, \sigma_K, \dots]) \mathbf{V}^T$$

where \mathbf{Q}, \mathbf{V} are unitary and $\sigma_1 \geq \sigma_2 \geq \dots \geq 0$. We then define

$$\mathbf{\Phi} = \underbrace{\text{diag}\left(\left[\frac{1}{\sigma_1}, \dots, \frac{1}{\sigma_K}\right]\right)}_{\mathbf{P}} \mathbf{Q}^T \mathbf{\Phi}_{\text{full}}$$

where the cutoff K is found by looking for a corner in the plot of σ_i vs i .

The approach in [5] approximates $\mathbf{\Phi}$ with a spectral method. In contrast, we compute $\mathbf{\Phi}_{\text{full}}$ analytically, and then leverage the SVD of $\mathbf{\Phi}$ to apply the same linear operators, $\mathbf{\Phi} = \mathbf{P}\mathbf{\Phi}_{\text{full}}$, to obtain a result that only has error from numerical precision, leading to slightly better numerical integration error than in [5].

Appendix B. Highlighting the Effects of Linearity in Parameters

When \mathbf{f} is linear in \mathbf{p} then then we can write the residual as follows:

$$\mathbf{r}(\mathbf{p}; \mathbf{U}, \mathbf{t}) = \mathbf{G}(\mathbf{U}, \mathbf{t})\mathbf{p} - \mathbf{b}(\mathbf{U}) \quad (\text{B.1})$$

where $\mathbf{G}(\mathbf{U}, \mathbf{t}) \in \mathbb{R}^{KD \times J}$ is a matrix-valued function that is constant with respect to \mathbf{p} . This leads to simplifications in the derivative information which can improve computational efficiency.

In the linear case, the Jacobian of the weak form right-hand side with respect to the parameters is the matrix $\mathbf{G}(\mathbf{U}, \mathbf{t})$. Formally, $\nabla_{\mathbf{p}}\mathbf{g}(\mathbf{p}; \mathbf{U}, \mathbf{t}) = \mathbf{G}(\mathbf{U}, \mathbf{t})$. This also simplifies implies $\nabla_{\mathbf{p}}\nabla_u\mathbf{g}(\mathbf{p}; \mathbf{U}, \mathbf{t}) = \nabla_u\mathbf{G}(\mathbf{U}, \mathbf{t})$. We again drop explicit dependence on \mathbf{U} and \mathbf{t} for simplicity of notation. Feeding this into our existing expression for the gradient of the weak form negative logarithm, we have

$$\begin{aligned} \nabla_{\mathbf{p}}\ell(\mathbf{p}) &= 2\mathbf{G}^T\mathbf{S}(\mathbf{p})^{-1}(\mathbf{G}\mathbf{p} - \mathbf{b}) \\ &\quad + (\mathbf{G}\mathbf{p} - \mathbf{b})^T(\partial_{\mathbf{p}_j}\mathbf{S}(\mathbf{p})^{-1})(\mathbf{G}\mathbf{p} - \mathbf{b}). \end{aligned}$$

Also, notice that $\mathbf{S}(\mathbf{p})$ now becomes quadratic in \mathbf{p} :

$$\mathbf{S}(\mathbf{p}) = (\nabla_u\mathbf{G}[\mathbf{p}] + \mathbf{\Phi} \otimes \mathbb{I}_D)(\Sigma \otimes \mathbb{I}_{M+1})(\nabla_u\mathbf{G}[\mathbf{p}] + \mathbf{\Phi} \otimes \mathbb{I}_D)^T$$

In fact $\nabla_u\mathbf{G}$ is the Jacobian of a matrix-valued function, and thus it is a three-dimensional tensor in $\mathbb{R}^{KD \times MD \times J}$. We treat it as a linear operator acting on \mathbf{p} . In practice this is a page-wise mat-vec across the third dimension of $\nabla_u\mathbf{G}$.

This causes the following simplification in the derivative of $\mathbf{S}(\mathbf{p})$:

$$\partial_{\mathbf{p}_j}\mathbf{S}(\mathbf{p}) = 2\nabla_u\mathbf{G}[\mathbf{e}_j](\Sigma \otimes \mathbb{I}_{M+1})(\nabla_u\mathbf{G}[\mathbf{p}] + \mathbf{\Phi} \otimes \mathbb{I}_D)^T$$

where $\mathbf{e}_j \in \mathbb{R}^J$ is the j^{th} canonical basis vector. This is equivalent to indexing into the j^{th} page of $\nabla_u\mathbf{G}$.

The second order derivative computations also simplify beyond the evaluation of $\mathbf{S}(\mathbf{p})$. Critically, observe that several terms in the Hessian are now guaranteed to be $\mathbf{0}$. In particular, we have $\forall \mathbf{p}$:

$$\partial_{\mathbf{p}_i, \mathbf{p}_j}\mathbf{G}\mathbf{p} = \mathbf{0} \in \mathbb{R}^J \text{ and } \partial_{\mathbf{p}_i, \mathbf{p}_j}\nabla_u\mathbf{G}[\mathbf{p}] = \mathbf{0} \in \mathbb{R}^{KD \times MD}.$$

Furthermore because $\nabla_u \mathbf{G}$ is constant with respect to \mathbf{p} , then $\partial_{\mathbf{p}_i \mathbf{p}_j} \mathbf{S}(\mathbf{p})^{-1}$ is constant with respect to \mathbf{p} , so this can be computed once and then reused.

Appendix C. Iterative Re-weighted Least Squares

In the previous work [5], the covariance information was incorporated by solving the generalized least squares problem

$$\hat{\mathbf{p}} = \underset{\mathbf{p} \in \mathbb{R}^J}{\operatorname{argmin}} (\mathbf{g}(\mathbf{p}; \mathbf{U}, \mathbf{t}) - \mathbf{b}(\mathbf{U}))^T \mathbf{S}(\mathbf{p}^*; \mathbf{U})^{-1} (\mathbf{g}(\mathbf{p}; \mathbf{U}, \mathbf{t}) - \mathbf{b}(\mathbf{U})).$$

Because $\mathbf{S}(\mathbf{p}^*; \mathbf{U})$ is not known, it has to be approximated with the current value of \mathbf{p} . This gives rise the iterative re-weighted least squares algorithm, which iterates as follows

$$\hat{\mathbf{p}}^{(i+1)} = \underset{\mathbf{p} \in \mathbb{R}^J}{\operatorname{argmin}} (\mathbf{g}(\mathbf{p}) - \mathbf{b})^T \mathbf{S}(\hat{\mathbf{p}}^{(i)})^{-1} (\mathbf{g}(\mathbf{p}) - \mathbf{b}) \quad (\text{C.1})$$

until the iterates are sufficiently close together (and again, we drop explicit dependence on \mathbf{U} and \mathbf{t}). This iteration involves computing the covariance estimate $\mathbf{S}(\mathbf{p})$ then solving a weighted least squares problem. The previous work [5] only considered problems that were linear in parameters, so in the nonlinear case, we have extended this algorithm by solving a nonlinear weighted least squares problem at each iteration where the Jacobian is computed using analytic derivative information described in Equations (7) and (8).

The previous work also chose the same initial guess based on the ordinary least square solution:

$$\hat{\mathbf{p}}^{(0)} = \underset{\mathbf{p} \in \mathbb{R}^J}{\operatorname{argmin}} \frac{1}{2} \|\mathbf{g}(\mathbf{p}) - \mathbf{b}\|_2^2$$

When the ODE was linear, this was done explicitly through the linear algebra. In the nonlinear case, this can no longer be done, so an initial guess is necessary. In this work, we pass all algorithms the same initial guess that is randomly sampled from parameter range specified in Table 2.

Appendix D. Supplemental Material

Appendix D.1. Plots

The following plots give detailed information on the bias, variance, MSE and coverage for all parameters for all ODEs, grouped by noise level.



Figure D1: Left: the squared bias, variance and MSE for p_1 (top) and p_2 (bottom), as a function of noise level. Right: the coverage levels for p_1 (top) and p_2 (bottom), as a function of noise level.

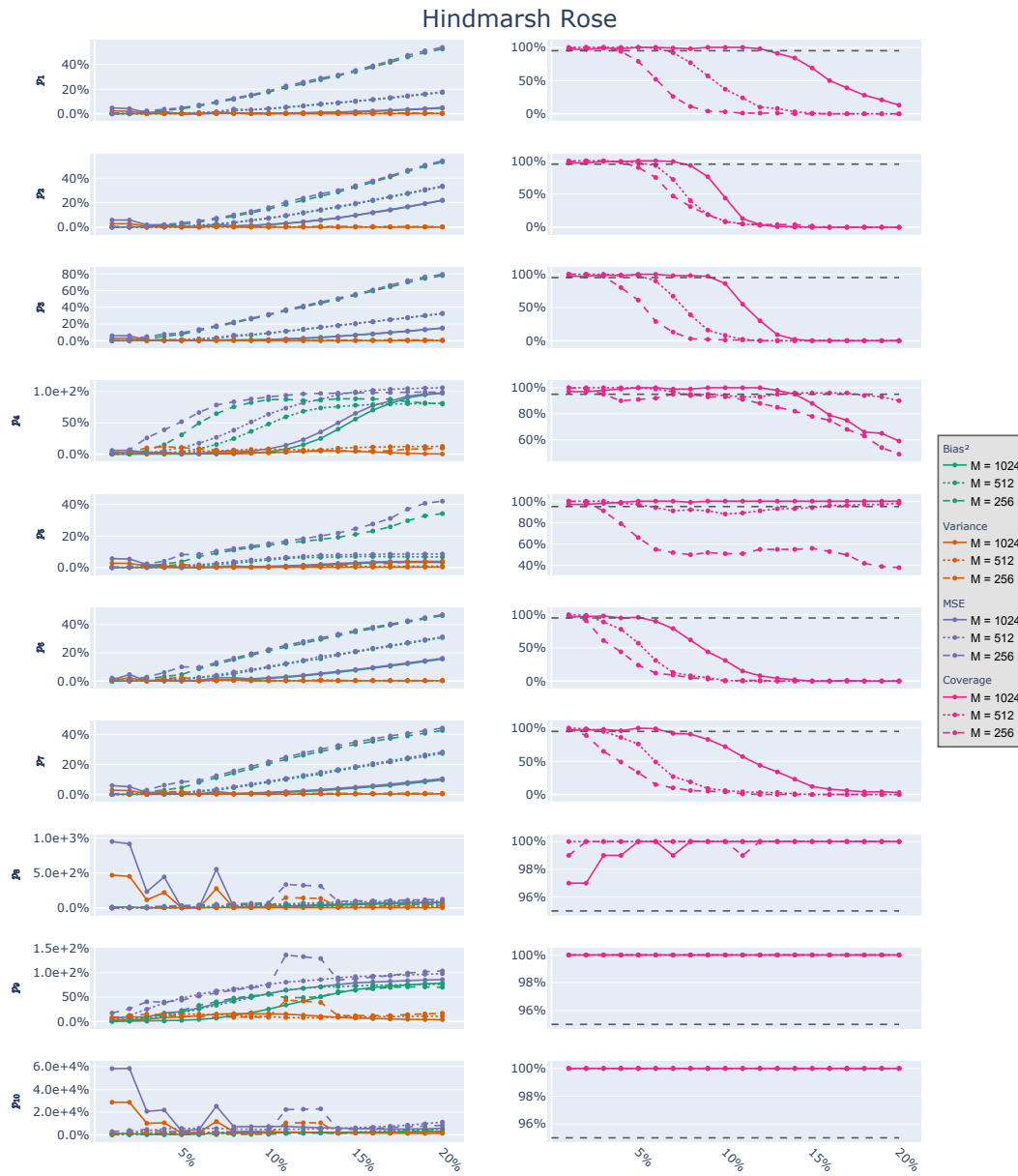


Figure D2: Left: the squared bias, variance and MSE for $p_1 - p_{10}$ top to bottom respectively, as a function of noise level. Right: the coverage levels for $p_1 - p_{10}$ top to bottom respectively, as a function of noise level.

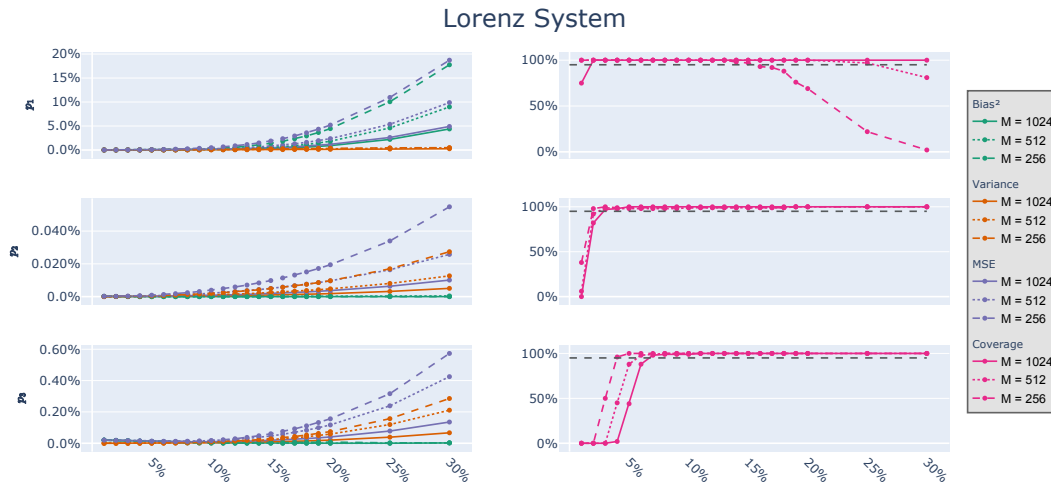


Figure D3: Left: the squared bias, variance and MSE for $p_1 - p_3$ top to bottom respectively, as a function of noise level. Right: the coverage levels for $p_1 - p_3$ top to bottom respectively, as a function of noise level.

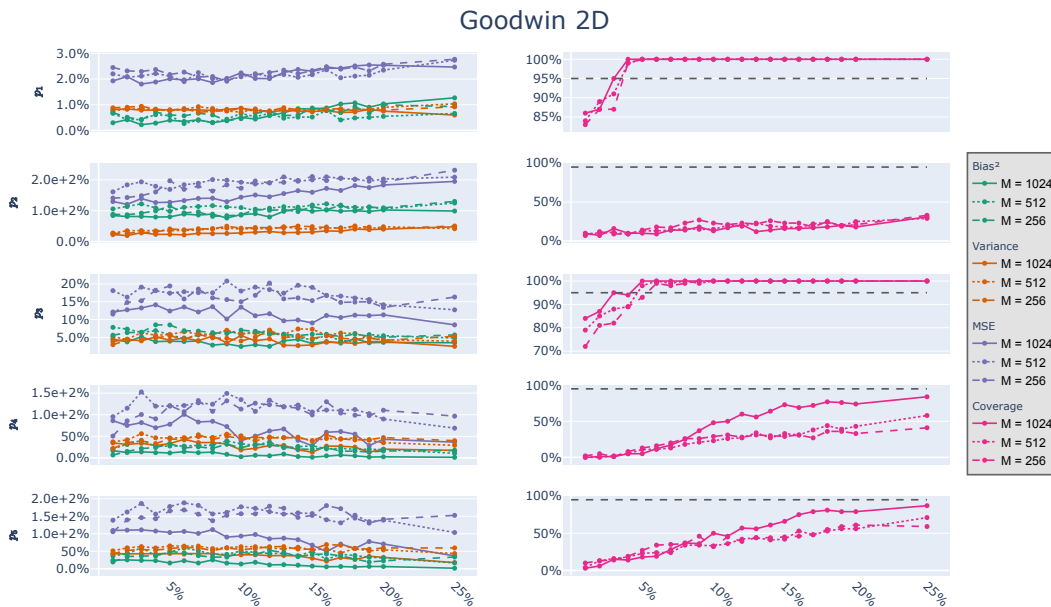


Figure D4: Left: the squared bias, variance and MSE for $p_1 - p_5$ top to bottom respectively, as a function of noise level. Right: the coverage levels for $p_1 - p_5$ top to bottom respectively, as a function of noise level.

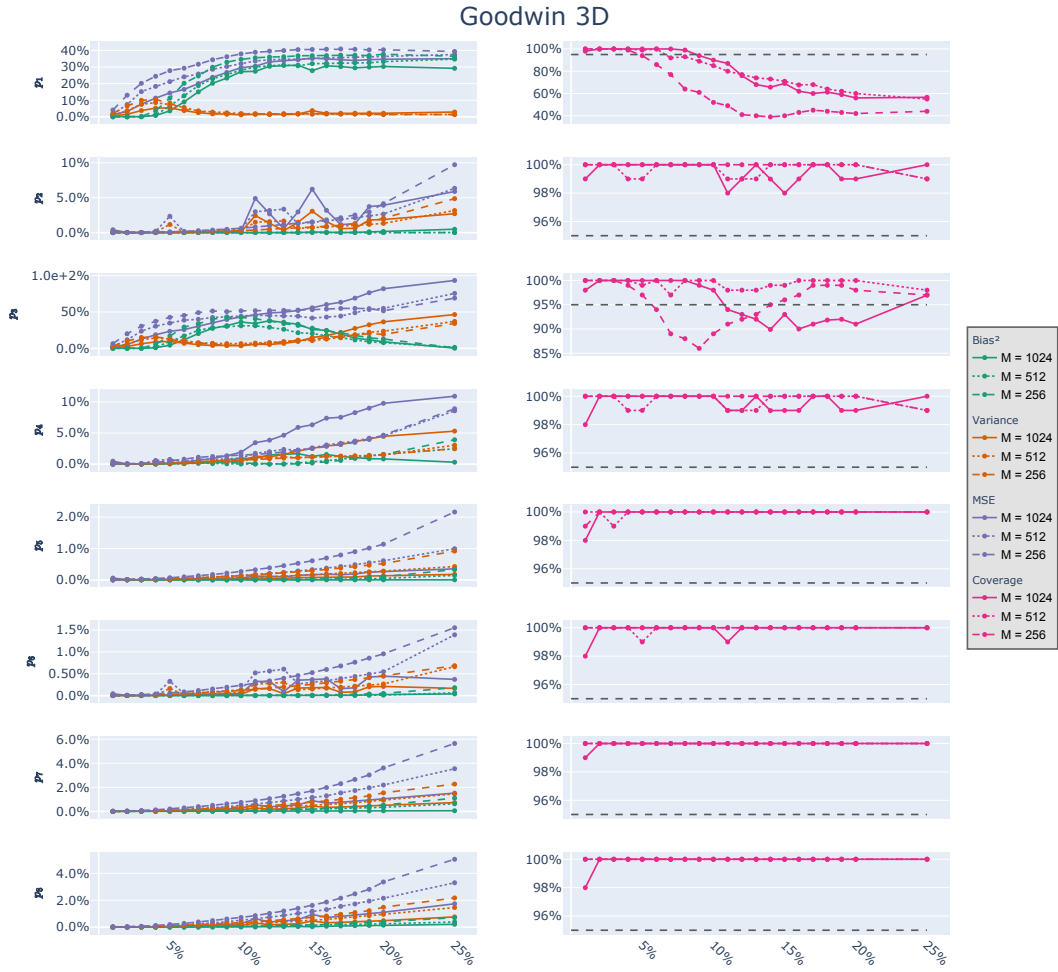


Figure D5: Left: the squared bias, variance and MSE for $p_1 - p_8$ top to bottom respectively, as a function of noise level. Right: the coverage levels for $p_1 - p_8$ top to bottom respectively, as a function of noise level.

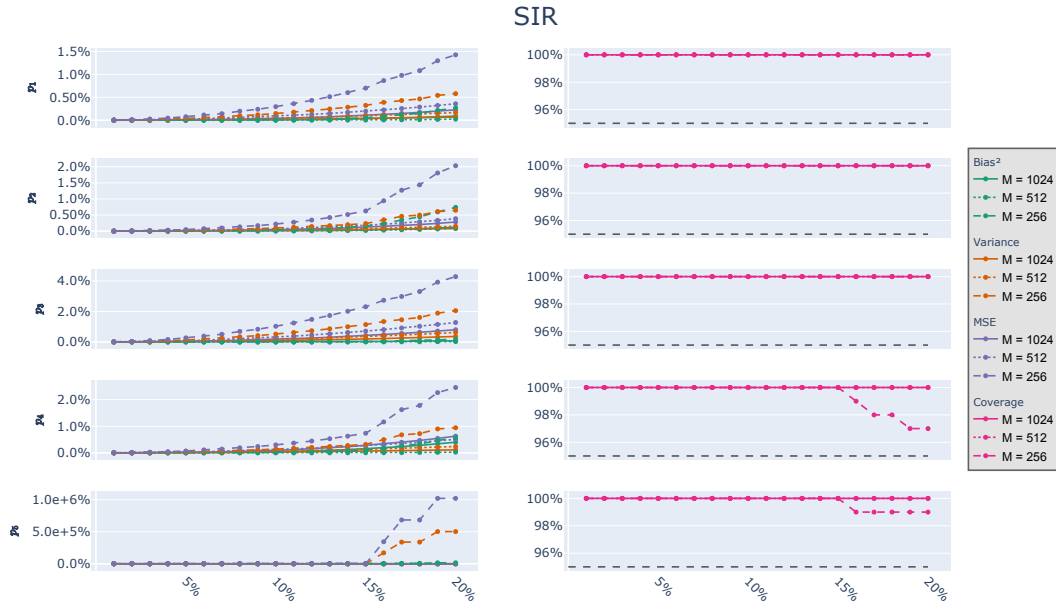


Figure D6: Left: the squared bias, variance and MSE for $p_1 - p_5$ top to bottom respectively, as a function of noise level. Right: the coverage levels for $p_1 - p_5$ top to bottom respectively, as a function of noise level.

Appendix D.2. Tables

The following tables give detailed information on the bias, variance, MSE and coverage for all parameters for all ODEs, grouped by noise level.

Table D8: Lorenz (continued)

		25%			30%		
		M=1000	M=500	M=250	M=1000	M=500	M=250
p_1	Bias	-1.5	-2.1	-3.2	-2.1	-3	-4.2
	Variance	0.2	0.38	0.45	0.26	0.45	0.48
	MSE	2.6	5.4	11	4.9	9.9	19
	Coverage	1	0.97	0.22	1	0.81	0.02
p_2	Bias	0.0033	0.048	0.0078	-0.00046	0.057	-0.0038
	Variance	0.025	0.063	0.13	0.04	0.099	0.21
	MSE	0.05	0.13	0.27	0.079	0.2	0.43
	Coverage	1	1	1	1	1	1
p_3	Bias	-0.0056	-0.0011	0.014	-0.012	-0.015	-0.012
	Variance	0.0028	0.0085	0.011	0.0047	0.015	0.02
	MSE	0.0055	0.017	0.022	0.0096	0.03	0.041
	Coverage	1	1	1	1	1	1

Table D10: Goodwin 2D (continued)

		16%			17%			18%			19%			20%					
		M=1024	M=512	M=256	M=1024	M=512	M=256	M=1024	M=512	M=256	M=1024	M=512	M=256	M=1024	M=512	M=256			
p_1	Bias	-6.7	-6.4	-6.5	-7.3	-4.6	-6	-7.5	-5	-6.9	-6.9	-5.1	-5.9	-7.3	-5.3	-7.2			
	Variance	40	41	43	36	43	44	37	42	40	43	43	43	39	47	41			
	MSE	1.3e+02	1.2e+02	1.3e+02	1.3e+02	1.1e+02	1.2e+02	1.3e+02	1.1e+02	1.3e+02	1.3e+02	1.1e+02	1.2e+02	1.3e+02	1.2e+02	1.3e+02			
	Coverage	1	1	1	1	1	1	1	1	1	1	1	1	1	1	1			
p_2	Bias	1	1.1	1	0.99	1.1	1.1	1	1.1	1	0.99	1.1	1.1	1	1	1			
	Variance	0.35	0.44	0.47	0.34	0.45	0.44	0.41	0.46	0.51	0.39	0.42	0.47	0.4	0.48	0.42			
	MSE	1.7	2.1	2	1.7	2	2.1	1.8	2	2	1.8	2	2.1	1.8	2	1.9			
	Coverage	0.16	0.17	0.23	0.17	0.22	0.18	0.18	0.24	0.25	0.2	0.2	0.19	0.18	0.25	0.21			
p_3	Bias	-0.39	-0.47	-0.48	-0.37	-0.41	-0.46	-0.43	-0.39	-0.49	-0.37	-0.48	-0.46	-0.38	-0.47	-0.45			
	Variance	0.15	0.23	0.22	0.14	0.25	0.19	0.13	0.24	0.18	0.15	0.2	0.19	0.15	0.17	0.17			
	MSE	0.45	0.67	0.67	0.42	0.66	0.59	0.45	0.64	0.6	0.44	0.63	0.6	0.45	0.57	0.54			
	Coverage	1	1	1	1	1	1	1	1	1	1	1	1	1	1	1			
p_4	Bias	0.22	0.46	0.49	0.26	0.47	0.39	0.22	0.45	0.4	0.14	0.45	0.37	0.16	0.44	0.4			
	Variance	0.27	0.45	0.53	0.27	0.44	0.44	0.25	0.46	0.42	0.13	0.41	0.42	0.2	0.35	0.47			
	MSE	0.59	1.1	1.3	0.61	1.1	1	0.55	1.1	0.99	0.29	1	0.98	0.43	0.9	1.1			
	Coverage	0.69	0.31	0.31	0.72	0.38	0.27	0.77	0.44	0.36	0.76	0.39	0.36	0.74	0.43	0.33			
p_5	Bias	0.23	0.52	0.65	0.25	0.64	0.61	0.22	0.62	0.53	0.26	0.57	0.44	0.25	0.56	0.47			
	Variance	0.22	0.57	0.69	0.32	0.45	0.67	0.27	0.58	0.58	0.36	0.51	0.56	0.32	0.54	0.59			
	MSE	0.49	1.4	1.8	0.71	1.3	1.7	0.58	1.5	1.4	0.78	1.3	1.3	0.71	1.4	1.4			
	Coverage	0.75	0.53	0.46	0.79	0.48	0.48	0.81	0.53	0.55	0.79	0.56	0.59	0.79	0.56	0.61			
		25%																	
		M=1024	M=512	M=256															
p_1	Bias	-8.1	-5.9	-6.9															
	Variance	31	54	48															
	MSE	1.3e+02	1.4e+02	1.4e+02															
	Coverage	1	1	1															
p_2	Bias	1	1.1	1.1															
	Variance	0.48	0.42	0.51															
	MSE	2	2.1	2.3															
	Coverage	0.31	0.29	0.33															
p_3	Bias	-0.37	-0.44	-0.48															
	Variance	0.1	0.16	0.21															
	MSE	0.34	0.51	0.65															
	Coverage	1	1	1															
p_4	Bias	0.12	0.33	0.41															
	Variance	0.18	0.29	0.4															
	MSE	0.36	0.69	0.97															
	Coverage	0.84	0.58	0.41															
p_5	Bias	0.12	0.41	0.58															
	Variance	0.18	0.43	0.6															
	MSE	0.37	1	1.5															
	Coverage	0.87	0.71	0.59															

Table D13: Goodwin 3D (continued)

		25%		
		M=1024	M=512	M=256
p_1	Bias	-1.9	-2.1	-2.1
	Variance	0.35	0.17	0.17
	MSE	4.3	4.6	4.8
	Coverage	0.57	0.55	0.44
p_2	Bias	0.0067	0.00089	0.00025
	Variance	0.00025	0.0003	0.00046
	MSE	0.00055	0.0006	0.00091
	Coverage	1	0.99	0.99
p_3	Bias	-0.055	-0.12	-0.087
	Variance	0.47	0.37	0.34
	MSE	0.93	0.76	0.69
	Coverage	0.97	0.98	0.97
p_4	Bias	0.55	-1.6	-2
	Variance	5.3	3.1	2.5
	MSE	11	8.6	8.9
	Coverage	1	0.99	0.99
p_5	Bias	-0.00035	0.0037	0.0056
	Variance	1.6e-05	4e-05	8.6e-05
	MSE	3.3e-05	9.3e-05	0.0002
	Coverage	1	1	1
p_6	Bias	0.0012	0.0015	0.0025
	Variance	5.6e-06	2.2e-05	2.3e-05
	MSE	1.3e-05	4.7e-05	5.2e-05
	Coverage	1	1	1
p_7	Bias	0.0022	0.0077	0.01
	Variance	6.9e-05	0.00014	0.00021
	MSE	0.00014	0.00033	0.00053
	Coverage	1	1	1
p_8	Bias	0.0036	0.0048	0.0065
	Variance	4.6e-05	8.8e-05	0.00013
	MSE	0.0001	0.0002	0.0003
	Coverage	1	1	1

Table D15: Goodwin 3D (continued)

		25%		
		M=1024	M=512	M=256
p_1	Bias	-1.9	-2.1	-2.1
	Variance	0.35	0.17	0.17
	MSE	4.3	4.6	4.8
	Coverage	0.57	0.55	0.44
p_2	Bias	0.0067	0.00089	0.00025
	Variance	0.00025	0.0003	0.00046
	MSE	0.00055	0.0006	0.00091
	Coverage	1	0.99	0.99
p_3	Bias	-0.055	-0.12	-0.087
	Variance	0.47	0.37	0.34
	MSE	0.93	0.76	0.69
	Coverage	0.97	0.98	0.97
p_4	Bias	0.55	-1.6	-2
	Variance	5.3	3.1	2.5
	MSE	11	8.6	8.9
	Coverage	1	0.99	0.99
p_5	Bias	-0.00035	0.0037	0.0056
	Variance	1.6e-05	4e-05	8.6e-05
	MSE	3.3e-05	9.3e-05	0.0002
	Coverage	1	1	1
p_6	Bias	0.0012	0.0015	0.0025
	Variance	5.6e-06	2.2e-05	2.3e-05
	MSE	1.3e-05	4.7e-05	5.2e-05
	Coverage	1	1	1
p_7	Bias	0.0022	0.0077	0.01
	Variance	6.9e-05	0.00014	0.00021
	MSE	0.00014	0.00033	0.00053
	Coverage	1	1	1
p_8	Bias	0.0036	0.0048	0.0065
	Variance	4.6e-05	8.8e-05	0.00013
	MSE	0.0001	0.0002	0.0003
	Coverage	1	1	1

Table D17: SIR-TDI (continued)

		16%			17%			18%			19%			20%		
		M=1024	M=512	M=256	M=1024	M=512	M=256	M=1024	M=512	M=256	M=1024	M=512	M=256	M=1024	M=512	M=256
p_1	Bias	-0.004	-0.0015	-0.0058	-0.0045	-0.0018	-0.0069	-0.005	-0.0022	-0.0078	-0.0055	-0.0026	-0.0093	-0.006	-0.003	-0.01
	Variance	1.7e-05	4.4e-05	0.00016	1.9e-05	4.9e-05	0.00017	2.2e-05	5.5e-05	0.00019	2.5e-05	6.1e-05	0.00022	2.7e-05	6.7e-05	0.00023
	MSE	5e-05	9e-05	0.00035	5.9e-05	0.0001	0.00039	6.9e-05	0.00011	0.00043	7.9e-05	0.00013	0.00052	9.1e-05	0.00014	0.00057
	Coverage	1	1	1	1	1	1	1	1	1	1	1	1	1	1	1
p_2	Bias	0.032	0.026	0.073	0.036	0.03	0.089	0.041	0.035	0.1	0.046	0.039	0.12	0.052	0.044	0.13
	Variance	0.0011	0.002	0.0079	0.0013	0.0023	0.01	0.0014	0.0026	0.011	0.0016	0.003	0.014	0.0018	0.0034	0.015
	MSE	0.0032	0.0048	0.021	0.0039	0.0056	0.029	0.0046	0.0065	0.032	0.0054	0.0075	0.041	0.0064	0.0087	0.046
	Coverage	1	1	1	1	1	1	1	1	1	1	1	1	1	1	1
p_3	Bias	-0.0014	-0.00059	-0.0017	-0.0016	-0.00073	-0.0019	-0.0017	-0.00088	-0.0022	-0.0019	-0.001	-0.0028	-0.002	-0.0012	-0.0031
	Variance	1.2e-05	2.2e-05	7.4e-05	1.4e-05	2.5e-05	8e-05	1.6e-05	2.8e-05	8.8e-05	1.8e-05	3.1e-05	0.0001	2e-05	3.4e-05	0.00011
	MSE	2.7e-05	4.5e-05	0.00015	3.1e-05	5e-05	0.00016	3.5e-05	5.7e-05	0.00018	3.9e-05	6.3e-05	0.00021	4.4e-05	7e-05	0.00023
	Coverage	1	1	1	1	1	1	1	1	1	1	1	1	1	1	1
p_4	Bias	-0.0049	-0.00089	-0.0046	-0.0055	-0.0011	-0.0058	-0.006	-0.0013	-0.0065	-0.0066	-0.0016	-0.0077	-0.0072	-0.0019	-0.0085
	Variance	9.4e-06	2e-05	6.3e-05	1e-05	2.2e-05	8.7e-05	1.2e-05	2.5e-05	9.2e-05	1.3e-05	2.8e-05	0.00011	1.5e-05	3.1e-05	0.00012
	MSE	4.3e-05	4e-05	0.00015	5.1e-05	4.5e-05	0.00021	6e-05	5.1e-05	0.00023	6.9e-05	5.8e-05	0.00029	8e-05	6.5e-05	0.00031
	Coverage	1	1	0.99	1	1	0.98	1	1	0.98	1	1	0.97	1	1	0.97
p_5	Bias	0.00012	-2.1e-05	0.01	0.00013	-2.1e-05	0.02	0.00014	-2e-05	0.02	0.00015	-1.8e-05	0.03	0.00016	-1.6e-05	0.03
	Variance	3.5e-09	6.8e-09	0.0099	4.1e-09	7.7e-09	0.02	4.6e-09	8.7e-09	0.02	5.3e-09	9.7e-09	0.029	6e-09	1.1e-08	0.029
	MSE	2.1e-08	1.4e-08	0.02	2.4e-08	1.6e-08	0.039	2.8e-08	1.8e-08	0.039	3.2e-08	2e-08	0.059	3.7e-08	2.2e-08	0.059
	Coverage	1	1	0.99	1	1	0.99	1	1	0.99	1	1	0.99	1	1	0.99